

**THE FATIGUE STRENGTH OF STIFFENER DETAILS
FABRICATED WITH SUBSTANDARD WELDS**

By

PAUL G. POYNTER

Bachelor of Science

Oklahoma State University

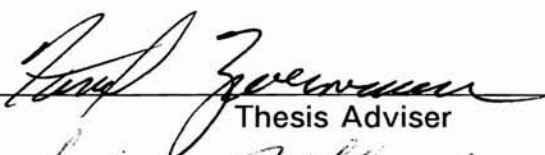
Stillwater, Oklahoma

1993

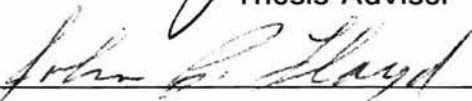
**Submitted to the Faculty of the
Graduate College of the
Oklahoma State University
in partial fulfillment of
the requirements for
the Degree of
MASTER OF SCIENCE
May, 1995**


THE FATIGUE STRENGTH OF STIFFENER DETAILS
FABRICATED WITH SUBSTANDARD WELDS

Thesis Approved:



Thesis Adviser







Dean of the Graduate College

ACKNOWLEDGMENTS

I express my sincere appreciation to the faculty and staff in the School of Civil and Environmental Engineering for their instruction and assistance throughout my academic career at Oklahoma State University. I am especially beholden to my major advisor, Dr. Farrel J. Zwerneman. His guidance, assistance, encouragement, and friendship have been invaluable not only on this research but also throughout my academic career. Additionally, I am most appreciative of my committee members, Dr. John P. Lloyd and Dr. Timothy D. Hogue. Their lessons have served me well and will be with me always. Finally, I thank Dr. Robert K. Hughes for his counsel and opportunities for financial assistance.

TABLE OF CONTENTS

Chapter	Page
I. INTRODUCTION	1
1.1 Background	1
1.2 Objectives	3
1.3 Scope	4
II. LITERATURE SURVEY.....	5
2.1 Weld Quality	5
2.2 Studies on Fatigue Strength	11
2.3 Improving the Fatigue Strength of Welded Joints.....	19
2.4 Calculated and Actual Bridge Response.....	22
2.5 Fatigue Evaluation Procedures	25
III. EXPERIMENTAL PROGRAM	36
3.1 Specimen Preparation	36
3.2 Test Setup.....	46
3.3 Test Procedures	50
3.4 Results and Discussion	53
IV. ESTIMATE OF REMAINING FATIGUE LIFE	64
V. SUMMARY AND CONCLUSIONS	70
5.1 Summary.....	70
5.2 Conclusions	71
REFERENCES	72

LIST OF TABLES

Table	Page
1. Fusion Weld Discontinuities	6
2. Fraction of Trucks in Outer Lane.....	34
3. Observed Average Daily Traffic (ADT) Growth Rates.....	35
4. Fatigue Test Data.....	58

LIST OF FIGURES

Figure	Page
1. Fillet Weld Discontinuities in a T-Joint	7
2. Fillet Weld Profiles	12
3. AASHTO Fatigue Resistance Curve for Category C Detail	17
4. West German Test Data	18
5. Truck Volume Ratio (T_a/T)	32
6. Longitudinal View of a Typical Test Specimen	37
7. Cross Section of a Typical Test Specimen	38
8. A Typical Welded Joint on the Control Specimen	40
9. Welding a Test Specimen	42
10. A Typical Welded Joint with Substandard Welds	44
11. Repaired Joint.....	45
12. Strain Gage Configuration.....	47
13. Simple Support	48
14. Load Configuration on Test Specimen.....	49
15. Test Setup	51

Figure	Page
16. Splice Plate Detail.....	54
17. A Typical Crack at a Stiffener Detail.....	56
18. Crack Surface at a Stiffener Detail	57
19. Comparison of the Control Specimen Test Data and the Fatigue Curve Generated by Fisher et al.	59
20. Plot of the Test Data for the Stiffener Details with Substandard Welds.....	60
21. Comparison of the Test Data to AASHTO Fatigue Curves for Category C and D Details.....	62

NOMENCLATURE

A	intercept of allowable stress range curve
A'	intercept of mean stress range curve
a	present age of bridge, years
b	slope of fatigue resistance curve
C	stress cycles per truck passage
f	ratio of mean stress range curve intercept and allowable stress range curve intercept
p_i	fraction of stress ranges within an interval
F_L	fraction of trucks in outer lane
F_T	fraction of trucks in traffic
F_{s1}	effective stress range modification factor
g	annual growth rate, %
K	fatigue curve intercept modification constant
N	number of load cycles to failure
R_s	reliability factor
R_{s0}	basic reliability factor
S_r	effective stress range, ksi
S_{ri}	midwidth of the stress range interval, ksi

- T present average daily truck volume in outer lane, trucks per day
- T_a lifetime average daily truck volume in outer lane, trucks per day
- Y_f remaining fatigue life, years

CHAPTER I

INTRODUCTION

1.1 Background

In Pittsburgh County, Oklahoma on the west side of Lake Eufaula, U.S. Highway 69 crosses the South Canadian River. The bridge at this location was widened by closing the gap between the north and southbound spans and by outwardly extending the decks of both spans. The gap was closed by adding crossframes between existing interior girders. The decks were extended outward by widening the piers, adding one row of plate girders outside each span, and connecting crossframes between the added girders and the existing girders.

Difficulties were encountered while erecting the crossframes. As specified in the plans, the crossframes were to be welded to stiffeners on existing girders and bolted to stiffeners on added girders. It was soon discovered that the bolt holes in the crossframes did not correspond to the bolt holes in the stiffeners of the added girders. To accommodate the discrepancy in bolt holes, the crossframes were simply welded at all locations.

Unfortunately, welding of the crossframes was faulty. Erection took place while the bridge was under traffic; consequently, the girders experienced movement making it difficult for the welders to maintain an arc.

In addition, the welders used incorrect electrodes and failed to preheat. General welding technique was poor and weld quality suffered greatly.

Certainly, poor weld quality has been detrimental to the bridge. But, the fact that welding took place at unintended locations is of equal concern. Plans called for the crossframes to be welded to only the stiffeners on the existing girders leaving the flanges of the girders unaffected. In practice, the crossframes were welded not only to the stiffeners but also directly to the inside of the bottom flanges of both existing and added plate girders. Upon loading the bridge the bottom flange experiences tension at most of these unintended weld locations. Unfortunately, welding to a structural member in a tensile region reduces the fatigue life of that member.

The American Association of State Highway and Transportation Officials (AASHTO) fatigue design specifications are relevant. According to the AASHTO fatigue specifications, stiffeners and short 2-in. attachments are considered Category C details. Both the stiffener-to-plate girder weld and the weld made on the girder flange during erection of the crossframes would qualify as Category C details provided proper welding procedures had been used. Because of the substandard welding procedures used to attach the bridge details, the bridge details may have fatigue lives below Category C. If poor welding has substantially reduced the fatigue strength of the details below Category C, the calculated stress range may exceed the allowable stress range at numerous locations along the bridge. As a result the projected fatigue life of the bridge would fall below the design life.

An increase in the calculated fatigue life may be achieved by repairing the welds. Furthermore, the number of repair locations may be substantially reduced if actual rather than calculated stress ranges are used to determine fatigue strength. The calculated stress ranges are based on conservative

design assumptions and are expected to be higher than the actual stress ranges. Even a minor decrease in stress range could substantially increase the fatigue life of a structural member. Actual stress ranges can be determined by instrumenting the bridge with strain gages and monitoring strains under both ambient traffic and a known load.

Clearly, the problems plaguing the U.S. Highway 69 bridge are sufficient to warrant investigation. Substandard welding at unintended locations has most likely affected fatigue strength. Once the effect on fatigue strength has been quantitatively examined, the remaining fatigue life of the bridge can be determined and a suitable method of repairing the substandard welds may be recommended.

1.2 Objectives

There are three major objectives to this study. The first objective is to generate the fatigue resistance curve for transverse stiffener details fabricated with substandard welds. Curve data will be obtained from fatigue tests conducted in the laboratory on steel beams with welded transverse stiffeners. The type and extent of weld discontinuities on laboratory specimens is to be characteristic of those found on the U.S. Highway 69 bridge crossing the South Canadian River. The fatigue resistance curve will show stress range, S_r , plotted against number of load cycles, N , to failure. The second objective is to estimate the remaining fatigue life of the U.S. Highway 69 bridge. Estimation will make use of the fatigue resistance curve generated and specific site information provided by the Oklahoma Department of Transportation (ODOT). The fatigue life will be based on actual stress ranges encountered on the bridge. The third objective is to

evaluate a feasible method of repairing the substandard welds with the intent of prolonging fatigue life.

1.3 Scope

The research conducted involved fatigue testing three beams with welded transverse stiffeners. All beams were size W14 X 43, and all material was A36 structural steel. One-sided stiffeners were attached by fillet welding to the web and both flanges. For test control, one specimen was fabricated using quality welding techniques conforming to the ANSI/AASHTO/AWS D1.5 Bridge Welding Code. The remaining two specimens were fabricated with defective welds by employing substandard welding techniques. An attempt was made to repair the weld at one stiffener location by rotary burr and disc grinding. Bending stress ranges at the stiffener-to-tension flange weld varied from 12.7 ksi to 27.6 ksi. All testing was limited to constant amplitude cyclic loading without stress reversal.

The remaining fatigue life of the U.S. Highway 69 bridge was evaluated by examining the most critically stressed bridge detail. The evaluation procedures considered fatigue strength of the detail, actual stress range at the detail, and traffic volume on the bridge. Data used in the evaluation came from laboratory tests, field measurements, and ODOT.

CHAPTER II

LITERATURE SURVEY

2.1 Weld Quality

2.1.1 General

A welded joint must have sufficient quality to perform reliably throughout the service life of the structure of which it is a part. The level of quality obtained in a welded joint is greatly influenced by the base materials, the welding materials, and the fabrication process. Employing skilled welders, selecting proper welding materials, and specifying correct welding procedures will encourage quality; however, all welds will contain some discontinuities.

2.1.2 Weld Discontinuities

Various types and sizes of weld discontinuities exist; Table 1 presents the most common. The weld discontinuities are categorized as either procedure related or metallurgical. Both categories adversely affect the weld by introducing stress concentrations. In addition, metallurgical discontinuities may affect chemical properties such as corrosion resistance. The weld discontinuities may be found in the weld metal, the base metal, or the weld heat-affected zone [2]. The T-joint shown in Figure 1 depicts the weld discontinuities listed in Table 1.

Table 1. Fusion Weld Discontinuities

Type of Discontinuity	Identification
Procedure Related	
Undercut	UC
Incomplete Fusion	IF
Overlap	OL
Undersize	US
Slag Inclusions	SI
Metallurgical	
Porosity	P
Cracking	CR

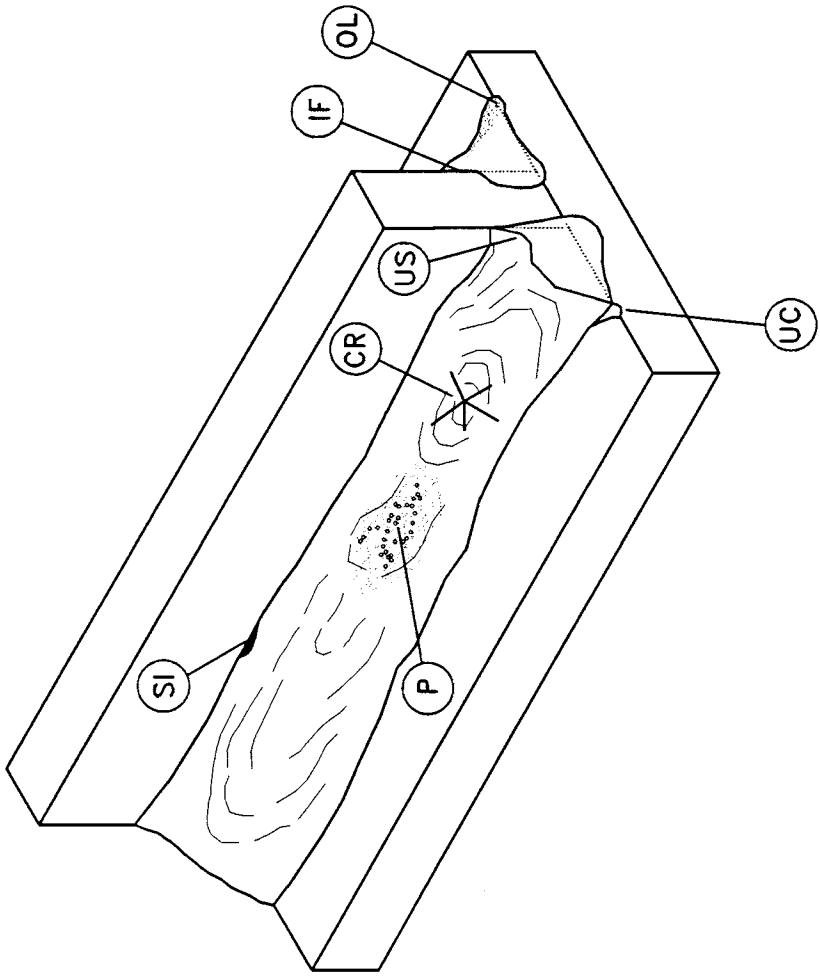


Figure 1. Fillet Weld Discontinuities in a T-Joint

Determining the type and extent of a discontinuity is the basis for judging weld quality. Below some acceptable level, the discontinuity is not considered harmful. Above that level, the discontinuity is a defect. Acceptable levels are generally determined by code specifications. Most notable is the ANSI/AWS Structural Welding Code [3]. These specifications permit latitude by defining a tolerance for weld discontinuities. The tolerance levels are based on experience and engineering judgment. During inspection, the extent to which a given discontinuity affects the size, shape, contour, and soundness of a weld is determined and compared to code provisions. Consequently, the inspector's understanding of the features and occurrences of weld discontinuities is paramount.

2.1.2.1 Undercut Undercut is the term used to describe a reduction in thickness of base metal. The reduction occurs at the edge of a bead of weld metal joining the surface of the base metal. Undercut is generally caused by improper welding technique; however, a high amperage and a long arc increase the tendency. Typically, the welder incorrectly manipulates the electrode while depositing weld material, and undercut results [4]. In addition to a reduction in cross-sectional area, the joint may experience local yielding at the tip of the undercut due to high stress concentrations. If excessive, undercut can materially reduce the strength of the joint. Strength reduction is most prevalent in joints subjected to severe fatigue conditions [21].

2.1.2.2 Incomplete Fusion The failure to fuse together adjacent layers of weld metal or weld metal and base metal is termed incomplete fusion. The welding arc must sufficiently penetrate the joint surfaces and raise the base

metal or previously deposited weld metal to the melting temperature or incomplete fusion will occur [20]. Penetration problems causing incomplete fusion can result from improper electrode manipulation or incorrect arc current. The electrode travel speed must not be too high, and the arc current must not be too low. Additionally, poor surface preparation causes incomplete fusion. Preweld cleaning must be sufficient to remove slag, oxides, or other foreign material [15].

2.1.2.3 Overlap The term overlap is used to describe a surface discontinuity that forms a severe mechanical notch parallel to the weld axis. Overlap is commonly caused by incorrect welding technique, wrong selection of welding materials, or improper preparation of the base metal. If slag, oxides, or other foreign matter on the base metal interfere with fusion, overlap may result along the toe, face, or root of the weld [2].

2.1.2.4 Undersize Undersize refers to a lack of welding material along the welded joint. It occurs when welding technique is poor. The welder simply fails to deposit enough weld material along the joint [2].

2.1.2.5 Slag Inclusions Non-metallic solid materials trapped in the weld metal or at the weld metal interfaces are termed slag inclusions. Many chemical reactions occur in the weld metal during deposition and subsequent solidification. Because of their lower specific gravity, non-metallic reaction products which are insoluble in molten metal will rise to the surface of the weld metal unless they become entrapped. The reaction products or slag may become entrapped below the surface of the molten metal by the stirring action of the arc. Slag may also follow ahead of the

arc if the welder manipulates the electrode incorrectly. Thus, slag inclusions can be prevented by employing good welding techniques [4].

2.1.2.6 Porosity Porosity is the presence of small voids in the weld material. The voids are created from gas being entrapped in the weld material during solidification. The voids may be either uniformly scattered throughout the weld or exist in localized clusters. Void size varies widely. They may be so small as not to be detectable by radiography, or they may be holes of more than 3/16 of an inch in diameter [15]. Porosity is a function of the degree of supersaturation of the gas in the weld metal. Gases, typically hydrogen and nitrogen, enter the weld pool through air entrainment in the arc atmosphere. Incidence of porosity may be reduced by using dry electrodes low in hydrogen content. In addition, correct amperage and proper arc length are imperative [20].

2.1.2.7 Cracking Cracks can exist in both the weld metal and the base metal. Two types of cracks can occur in a welded joint. Cracks which are observed during welding while the weld metal is in a plastic condition are termed hot cracks. Hot cracks develop as the weld metal begins to solidify. Cracks occurring in the heat-affected zone material after the joint is cooled are termed cold cracks. Both forms of cracking are influenced by the degree of restraint opposing movement during weld shrinkage. In addition, solidification rate is influential since it determines the structure and impurity distribution of the weld metal that may eventually crack. Cracking may be lessened by increasing heat input and by using preheat. Increasing heat input avoids excessive hardening of the heat-affected zone and allows hydrogen to disperse. Using preheat will help avoid cold cracking in the

heat-affected zone by preventing the joint from cooling too fast. Preheat is particularly useful in thick (3/4-in.) sections of mild steel [15].

2.1.3 Weld Profile

In addition to the discontinuities discussed, the finished profile of a weld may also adversely affect the service performance of a joint. Poor profile may cause stress concentrations as well as contribute to the formation of incomplete fusion or slag inclusions [2]. Figure 2 shows desirable, acceptable, and unacceptable fillet weld profiles.

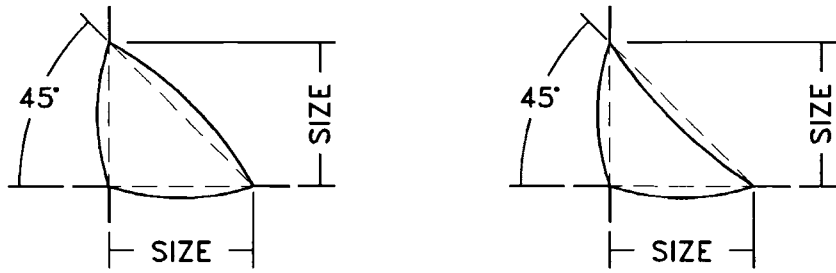
2.1.4 Effect of Weld Discontinuities on Fatigue Strength

Weld performance is greatly affected by the weld discontinuities discussed. Most particularly affected is fatigue strength. Fatigue cracks originate from notches producing a stress concentration under an applied stress. The majority of fatigue life of a weldment consists of crack propagation. Unfortunately, crack propagation rates are most significantly affected by stress concentrations. A given discontinuity serves only to increase any already existing stress concentration. Although all discontinuities may be significant in promoting fatigue failures, incomplete fusion, cracking, and undercut are the most detrimental. In addition to fusion weld discontinuities, weld profile defects can also seriously hinder fatigue performance by increasing stress concentrations [20].

2.2 Studies on Fatigue Strength

2.2.1 General

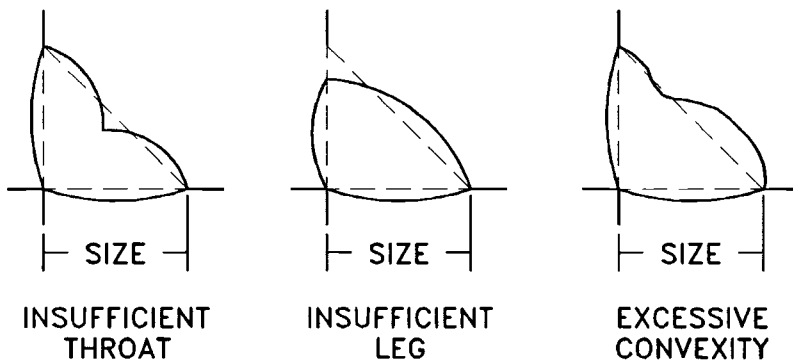
The current AASHTO Specifications [1] contain provisions for the fatigue



Desirable



Acceptable



Unacceptable

Figure 2. Fillet Weld Profiles

design of welded details on steel bridges. These provisions are based on fatigue resistance curves which reflect the expected fatigue life for a given stress range. Different curves exist for the different classes of welded details. Data accumulated from several major fatigue studies were used to generate the fatigue curves. The majority of data was obtained from extensive research sponsored by the National Cooperative Highway Research Program (NCHRP). In addition to fatigue testing over 800 full-sized welded steel bridge details, the fatigue studies sponsored by the NCHRP involved amassing the findings from several other fatigue studies conducted in the United States and abroad [12].

A substantial portion of the research conducted under the NCHRP concentrated on examining the fatigue strength of transverse stiffeners and similar attachments. Efforts to fatigue test transverse stiffeners welded to steel beams were aimed at developing the AASHTO fatigue resistance curve for Category C details. Under the NCHRP, quality testing was performed in which the variables influencing fatigue strength were properly controlled and measured. The test program is presented in NCHRP Report 147, *Fatigue Strength of Steel Beams with Welded Stiffeners and Attachments* [10].

2.2.2 NCHRP Test Procedures

A total of 47 beams with one-sided transverse stiffeners attached were tested in the NCHRP fatigue study. Multiple stiffeners were attached to each beam. Stiffener plates were manually fillet-welded to the beam web as well as the beam flanges. Normal fabrication techniques, workmanship, and inspection procedures conforming to the requirements of the ANSI/AASHTO/AWS D1.5 Bridge Welding Code were employed. To

simulate the restraint imposed by bridge diaphragms, lateral bracing was introduced at some stiffener locations causing an out-of-plane displacement proportional to the vertical displacement.

The two sizes of rolled steel beams studied were W14 X 30 and W10 X 25. These beam specimens were tested on simple supports with concentrated loads applied at two locations allowing for constant moment and moment gradient regions. The cyclic loading was applied through a hydraulic actuator operating at a frequency between 200 and 800 cycles per minute. Load was transmitted from the hydraulic actuator to the test beam through a spreader beam. The majority of tests involved no stress reversals, and all tests were limited to constant amplitude cyclic loading. Minimum flexural stress and flexural stress range at the stiffener-to-tension flange weld were the controlling variables. Tests were continued until cracks occurring at stiffener details reduced beam stiffness and allowed for an increase in deflection. After failure at one stiffener location, beam specimens were repaired by splicing across the cracked region, and testing was continued to produce failure at other stiffener locations.

2.2.3 NCHRP Findings

Test findings showed that the flexural stress range at the stiffener-to-tension flange weld was the dominant factor influencing fatigue strength. The minimum flexural stress at the stiffener-to-tension flange weld was insignificant. Furthermore, it was discovered that shear stresses did not affect fatigue strength. Thus, it was concluded that principal stresses and their direction need not be considered when designing stiffened bridge members. The attachment of diagonal bracing to the beam stiffeners had no

effect on fatigue strength, and out-of-plane bending at no time contributed to crack initiation or growth. Analysis of the crack growth indicated that the thickness of the flange and web was not a variable influencing the fatigue life of the stiffener details. The fatigue behavior examined in this study ranged between 10^5 and 10^7 cycles of loading. Furthermore, stiffeners welded to the web and flanges sustained 10.8 to 15.5 million load cycles at a stress range of 12 ksi without failure or visible crack growth.

All beam failures were the result of a large crack forming at the toe of the fillet weld connecting each stiffener to the tension flange. The large crack emerged from smaller cracks that initiated at several points along the toe of the weld. Propagating in a semielliptical shape, individual cracks grew and eventually joined. Once joined, the single crack front spread over most of the weld length before reaching the extreme fiber of the tension flange. After breaking through the extreme fiber, the crack grew across the tension flange and up into the web. Growing the cracks through the thickness of the flange consumed approximately 96 percent of the load cycles to failure. The likelihood of crack initiation and growth was greatest at locations subjected to a high tensile stress range and where initial micro-flaws existed. The initial micro-flaws were the result of discontinuities in the fillet weld. As suspected, the rate of crack propagation was proportional to the level of stress range as well as the extent of weld discontinuities.

2.2.4 AASHTO Fatigue Resistance Curve

The AASHTO fatigue resistance curve for a Category C detail was derived

from the NCHRP fatigue study on transverse stiffeners. The curve is presented in Figure 3. As previously noted, the fabrication techniques, workmanship, and inspection procedures employed in the NCHRP fatigue study complied with the ANSI/AASHTO/ AWS D1.5 Bridge Welding Code. This document places specific limits on cracking, convexity, undercut, lack of fusion, porosity, and undersizing. Such weld discontinuities are not considered weld defects until their size and frequency exceed the specified limits. The data obtained in the NCHRP fatigue study on transverse stiffeners applies to quality welds free of defects. Consequently, the AASHTO fatigue resistance curve for a Category C detail makes no allowance for substandard welding.

2.2.5 Fatigue Strength with Weld Defects

Information available on the fatigue strength of welded stiffeners containing weld defects is limited. In tests performed on beams with fillet welded stiffeners, Gurney [10, 14] attributed three early failures to undercut at the toe of the weld. Although the undercutting was slight, its presence reduced the fatigue life of the detail to below a Category C. In a West Germany study [12, 17], fatigue tests performed on welded stiffeners consistently yielded results that were significantly below the predicted strength. The reduced fatigue strength was reportedly due to unintended weld defects, namely hydrogen-induced cold cracking and weld undercutting. All the test data obtained in the West German study fell below the fatigue resistance curve for a Category C detail. A comparison of the test data obtained in the West German study to the AASHTO Category C fatigue resistance curve is shown in Figure 4.

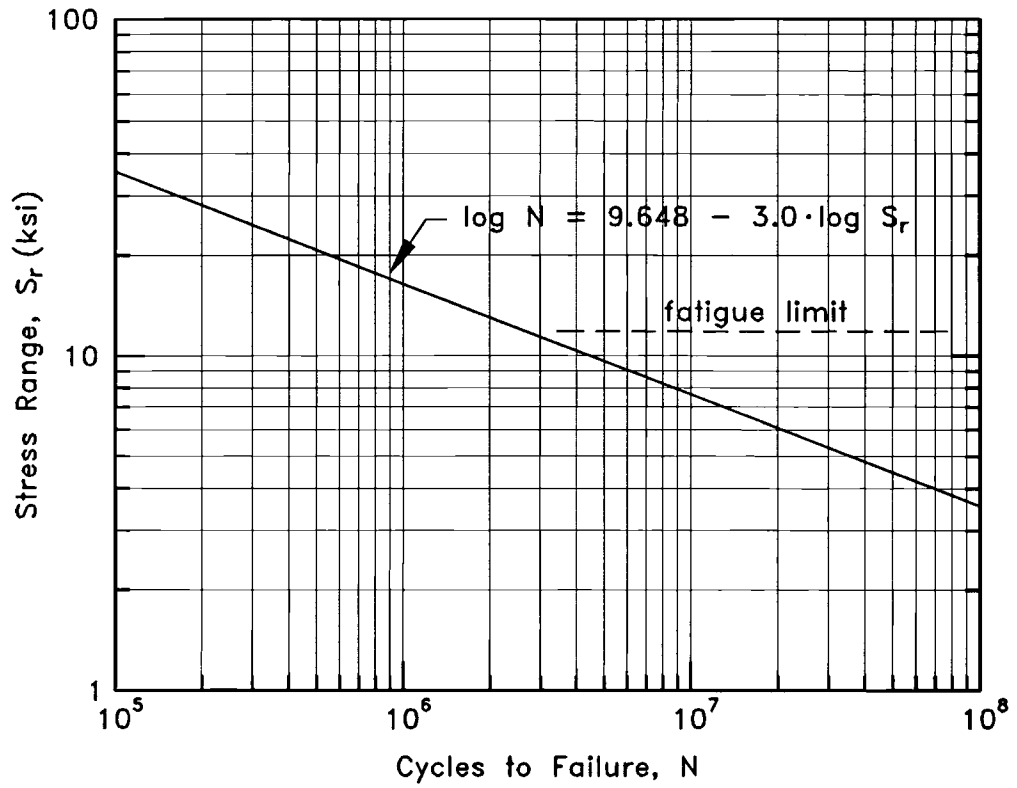


Figure 3. AASHTO Fatigue Resistance Curve for a Category C Detail

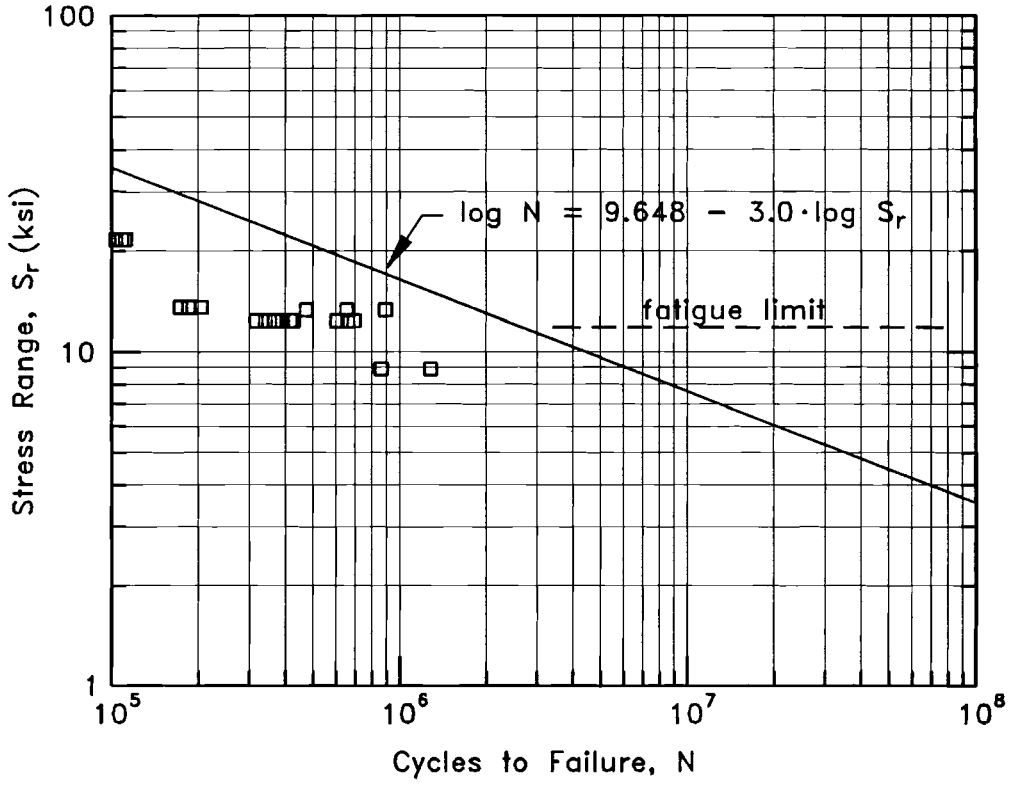


Figure 4. West German Test Data

2.3 Improving the Fatigue Strength of Welded Joints

2.3.1 General

It is known from previous fatigue studies [9, 10] on welded joints that fatigue cracks initiate and grow in areas subjected to a high tensile stress range where initial micro-flaws exist. In fillet welds, such as are used to attach transverse stiffeners, the initial micro-flaw condition is provided by discontinuities at the weld toe. The high tensile stress range is brought about by stress concentrations occurring at the weld toe. The tensile stress range may also be influenced by the presence of tensile residual stresses which result from the welding process. By lessening weld discontinuities, stress concentrations, and residual tensile stresses, the likelihood of crack initiation and growth can be reduced and fatigue strength can be improved.

2.3.2 Weld Modifying Techniques

A variety of techniques exist for modifying a welded joint and improving its fatigue strength. The most common and thoroughly examined techniques include grinding, remelting, and peening. The forms of grinding employed are usually either rotary burr or disc. Both forms of grinding reduce stress concentrations at the weld toe by altering the weld profile to achieve a smooth transition between the weld metal and the base metal. Grinding may also serve to reduce weld discontinuities such as undercut and slag inclusions.

Fatigue performance can also be improved by remelting. Remelting involves reducing the weld metal to a shallow depth along the weld toe. This process reduces slag inclusions and modifies weld profile, thereby reducing stress concentrations and crack initiation sites at the weld toe.

Another commonly used technique for improving fatigue performance is peening. Peening is a cold working process used to plastically deform the weld toe. Peening is usually accomplished by a high velocity stream of metal particles (shot peening) or by a tool (hammer peening). By peening, the weld toe profile is improved, thus reducing stress concentrations. Peening also hardens the weld and introduces residual compressive stresses; both functions can improve fatigue strength [13].

2.3.3 Studies on Grinding, Remelting, and Peening

In two National Cooperative Highway Research Program (NCHRP) studies [11, 13], the relative benefit of grinding, remelting, and peening was examined. In the NCHRP study conducted by Fisher et al., only a slight increase in the fatigue strength of joints with ground fillet weld toes was reported. The average increase in the fatigue life of ground joints over as-welded joints was less than 10 percent. Poor grinding techniques may have contributed to the lack of improvement in fatigue strength. On several specimens, the weld toe surface was damaged by the grinding burr; on one specimen, slag particles were not removed but rather covered by a layer of smeared metal.

Fisher et al. achieved the greatest success with remelting. Depending on stress range, increases in the fatigue life of details with remelted welds ranged from 270 to 360 percent. On some specimens, cracks initiated and propagated from the weld root demonstrating an upper bound to the improvements that are possible by remelting the weld toe.

Fisher et al. also found that peening the weld toe increases fatigue strength. The greatest increase in fatigue strength was observed in

specimens subjected to the highest stress ranges. Although peening blunted the crack-like slag inclusion and slowed crack initiation, fatigue cracks still eventually developed in the peened region at the weld toe.

When examining the same retrofitting techniques as Fisher et al., Gregory et al. concluded that toe grinding is the most practical and economical method of achieving a significant improvement in fatigue strength. The conflict in the researchers' results may stem from the fact that Gregory et al. primarily considered stress ranges near the fatigue limit, whereas Fisher et al. was concerned with higher stress ranges. Interestingly, the slight increase in the fatigue strength of ground joints that was reported by Fisher et al. occurred in the lowest stress range tests. It is worth noting that the American Welding Society Specification [3] also mentions remelting and peening but expresses a preference for grinding.

Gregory et al. further investigated the aspects of grinding by comparing disc and rotary burr grinding. It was found that disc grinding can be performed at almost twice the rate of burr grinding. However, burr grinding may be desirable because disc grinding suffers from two disadvantages. Being large and cumbersome, the disc grinder may be difficult to operate in tightly confined spaces. In addition, the operator of a disc grinder is more likely to remove too much material. In either case, the depth of grinding must be a minimum of $1/32$ in. beneath the plate surface. The maximum depth of grinding allowed is $5/64$ in. or 5 percent of the plate thickness. The final ground surfaces should be free from all traces of slag or undercut, and a smooth transition between the weld metal and the base metal should exist at the weld toe [13].

2.4 Calculated and Actual Bridge Response

2.4.1 General

The procedures used in design and analysis of highway bridges are inherently conservative. As a result, the actual response of a bridge often varies significantly from the calculated response. In reality, bridge stresses and particularly stress ranges are almost always lower than anticipated by calculations. Consequently, an analytical model used to estimate actual stress ranges must be developed from site specific data obtained from field measurements.

Structures with excessive strength stem from the designer's primary concern with safety and serviceability. During the design process, every effort is made to include safety factors to account for uncertainties in materials, loads, fabrication details, and possible construction errors. Procedures contained in the *AASHTO Standard Specifications for Highway Bridges* [1] are governed by a static strength design followed by fatigue checks. Because the strength design procedures must account for the worst conditions expected to occur over the life of the bridge, conservative assumptions are made in each step. Although these design procedures lead to bridge structures which are extraordinarily safe, these same procedures predict stress ranges which are far greater than actually felt by the structure [18].

In addition to conservative design assumptions, conservative analysis assumptions can also result in actual stresses being lower than calculated stresses. Analytical models of beam and slab bridges often fail to consider several ways in which load is resisted. In an investigation performed by

Burdette et al. [8], more than 50 years of bridge test data were collected and examined to determine specific load-resisting mechanisms that are typically not accounted for during design or evaluation. The investigation revealed that conservative analysis assumptions are made with regard to load distributions, composite action, and unintended continuity.

2.4.1.1 Load Distribution Load distribution refers to the lateral distribution of load to longitudinal supporting elements. How loads applied to the bridge deck distribute themselves laterally has a significant affect on the stress range experienced by each girder. Bridge tests indicate that the usual assumption that interior girders carry most of the load can be grossly conservative. A more realistic estimate of stress range is likely obtained by examining multiple load configurations nearer to exterior girders [8].

2.4.1.2 Composite Action The composite action of bridges with steel girders and concrete decks is generally underestimated. Tests on bridges with shear connectors frequently exhibit full composite action. Even in the absence of shear connectors several bridges have demonstrated some composite action. Bridges examined in the AASHTO Road Test [16] exhibited full composite action even after repeated stress cycles. In a study conducted by Viest et al. [22], steel beams with and without mechanical shear connectors were examined. In every test, complete interaction between slab and beam was observed so long as the bond between the concrete and steel flange remained unbroken. Though not quantitatively stated, these studies indicate that actual bridge stresses and stress ranges are lower than anticipated in design calculations.

2.4.1.3 Unintended Continuity Unintended continuity is the tendency of a bridge to act continuous at its simply supported ends. This action would undoubtedly result in actual stresses being lower than design stresses which do not consider resistance to end rotation. An analysis performed by Barton and McKeel [5] clearly showed that some allowance for end moment had to be made in order to match the bridge behavior measured in field tests. In a similar analysis performed by Burdette et al. [7], applying approximately 35 percent full fixity at the bridge ends resulted in a much closer matching of calculated and measured bridge response. Interestingly, these same results were observed in tests conducted by Buckle et al. [6].

2.4.2 Modeling

Incorrectly predicting actual bridge response is generally attributable to errors in modeling. Although the theories relied upon in structural analysis are accurate, the model being examined simply fails to reflect the actual characteristics of the bridge structure. As a result, models derived from test data taken at the bridge site are the most realistic [5]. In practice, bridge girders are fitted with strain gages at various locations. In particular, strain gages are placed along the lower flanges of all girders where maximum stress ranges are expected to occur. A known load closely resembling the real live load is moved on the bridge and strain measurements are taken for various positions of the static load.

Once actual bridge strains have been determined at specific locations, a finite element model of the bridge structure is generated. Before calibration, every effort is made to model the bridge structure as closely as possible. The model is then calibrated by adjusting the level of composite action at

the flange-deck interface, the moment restraint at the supports, and the load distribution on the deck until measured strains match calculated strains. Once the model is complete, it can be used to calculate the stresses at any point on the bridge, rather than being limited to just strain gage locations.

Several researchers [19] have obtained favorable results by performing variances of the procedures described above. Although quantifying how each of the different mechanisms affected actual response was practically impossible, generating a model which accurately predicted actual bridge response was possible. Furthermore, the models were successfully used to determine the stress ranges actually occurring on the bridge allowing for a more accurate estimate of fatigue life.

2.5 Fatigue Evaluation Procedures

2.5.1 General

Fatigue evaluation procedures for existing steel bridges were developed in a study sponsored by the NCHRP. The study collected information gained from several years of research on variable-amplitude fatigue response, high-cycle fatigue behavior, bridge detail fatigue strengths, actual traffic loadings, and bridge load distributions. This information was used to develop guidelines for calculating the remaining fatigue life of an existing bridge. These guidelines are presented in the NCHRP Report 299, *Fatigue Evaluation Procedures for Steel Bridges* [18].

2.5.2 NCHRP Evaluation Procedures

As specified in the NCHRP report, the remaining fatigue life for a bridge detail may be obtained by first determining a nominal stress range for the

truck traffic crossing the bridge. This stress range is then applied to a fatigue resistance curve generated from laboratory testing. The fatigue resistance curve reflects the number of load cycles a particular detail can sustain at a given stress range before failing. After determining the number of load cycles corresponding to this stress range, the life of the detail is calculated from an estimated truck volume and the present age of the bridge.

Two different procedures for estimating the remaining fatigue life of a detail are available. The two procedures are identified as remaining mean life and remaining safe life. Both estimates are calculated using the detail's fatigue data generated from laboratory tests. The remaining mean life estimate is based on the mean stress range curve. The mean stress range curve is developed from a linear regression analysis of the fatigue test data. The remaining safe life estimate is based on the allowable stress range curve. The allowable stress range curve is defined two standard deviations below the mean stress range curve. A standard deviation is calculated for the number of load cycles test data after transferring each of the values of the number of load cycles to same stress range value. These values are transferred using the slope of mean stress range curve. When determining the allowable stress range curve in this manner, it is assumed that the allowable stress range curve is parallel to the mean stress range curve on a log-log plot. Hence, the allowable stress range curve corresponds only approximately to the lower bound of the 95 percent confidence limit for the test data. The 95 percent confidence limit is the statistical limit which defines the interval of cycle life within which the fatigue test data occur 95 percent of the time.

The best possible estimate of the actual remaining life is reflected in the remaining mean life calculation. There is a 50 percent chance that the actual remaining life will exceed the remaining mean life. The remaining mean life is the same for redundant and nonredundant members.

A much higher degree of safety is provided by the remaining safe life calculation. In calculating the remaining safe life, different levels of safety are provided for redundant and nonredundant members. The probability that the actual remaining life will exceed the remaining safe life is 97.7 percent for redundant members and 99.9 percent for nonredundant members.

The fatigue life evaluation procedures derived from the NCHRP study were designed to provide consistent levels of reliability for different conditions. This is accomplished by providing basic procedures along with alternative procedures that may be better suited to the data available on a particular bridge. Although the alternative procedures may require more effort, they generally provide greater accuracy resulting in a longer calculated fatigue life. The NCHRP report provides an alternative procedure which relies on stress range measurements taken at the bridge site. This procedure is presented in the discussion that follows.

To calculate the remaining fatigue life for an estimated lifetime average daily truck volume, the following equation is used:

$$Y_f = \frac{f K X 10^6}{T_a C (R_s S_r)^b} - a \quad (2.1)$$

where Y_f = remaining fatigue life in years; S_r = effective stress range; R_s = reliability factor; C = stress cycles per truck passage; K , b , and f =

fatigue curve constants; T_a = estimated lifetime average daily truck volume; and a = present age of the bridge in years.

2.5.2.1 Effective Stress Range (S_r) In the general procedure, the nominal stress range is calculated from a rigorous analysis of the bridge structure. To determine the stress range, a model of the bridge structure is developed, and its response to a fatigue truck load is examined. As an alternative procedure, the effective stress range may be used. The effective stress range is calculated from stress-range histograms obtained from field measurements on the bridge under normal traffic. The histograms should reflect effective stress ranges at critical locations along the bridge. The effective stress range, S_r , for each histogram is calculated from the following equation:

$$S_r = (\sum p_i S_{ri}^3)^{1/3} \quad (2.2)$$

where p_i = fraction of stress ranges within an interval, and S_{ri} = midwidth of the interval.

2.5.2.2 Reliability Factor (R_s) The reliability factor is used to ensure an adequate level of safety. It is derived from a statistical analysis performed to determine the probability that the actual life will exceed the safe life. When determining the remaining safe life, multiply the computed stress range, S_r , by a reliability factor:

$$R_s = R_{s0}(F_{s1}) \quad (2.3)$$

where R_s = reliability factor associated with calculation of stress range; R_{s0} = basic reliability factor, 1.35 for redundant members and 1.75 for nonredundant members.

The effective stress range is considered more accurate if calculated using stress-range histograms. The factor, F_{s1} , accounts for this increased accuracy by reducing the effective stress range. Thus, if the effective stress range is calculated using stress-range histograms obtained from field measurements on the bridge, $F_{s1} = 0.85$. In all other cases, $F_{s1} = 1.0$. When determining the remaining mean life, $R_s = 1.0$.

2.5.2.3 Stress Cycles Per Truck Passage (C) The number of stress cycles per truck passage, C , can be determined from the values that follow:

For longitudinal members:

(a) Simple-span girders:

40-ft. or above = 1.0

Below 40-ft. = 1.8

(b) Continuous-span girders within a distance equal to 0.1 of the span on each side of an interior support:

80-ft. or above = $1 + (\text{span} - 80)/400$ in feet

40-ft. or above but below 80-ft. = 1.0

Below 40-ft. = 1.5

(c) Continuous-span girders elsewhere:

40-ft. or above = 1.0

Below 40-ft. = 1.5

(d) Cantilever (suspended span) girders = 2.0

(e) Trusses = 1.0

For transverse members:

(a) 20-ft. or above spacing = 1.0

(b) Below 20-ft. spacing = 2.0

2.5.2.4 Fatigue Curve Constants (K, b, and f) Data obtained from fatigue tests on laboratory specimens is used to evaluate the fatigue life of a particular type of detail. The fatigue test data consists of the number of load cycles, N , a detail can sustain at a given stress range, S_r , before failing. The relationship between the number of load cycles, N , and the stress range, S_r , has been determined from extensive test data obtained in fatigue studies sponsored by the NCHRP [12]. The relationship determined from the NCHRP fatigue studies is given by

$$NS_r^b = A \quad (2.4)$$

When plotted on a log-log scale, a straight line with an intercept A and a negative slope b is obtained. This straight line defines the fatigue resistance curve for the detail. In log form, the relationship is given by

$$\log N = \log A - b \cdot \log S_r \quad (2.5)$$

In the discussion that follows, the constant A is the intercept value of the allowable stress range fatigue curve. As previously discussed, the allowable stress range fatigue curve is used to calculate the remaining safe life and is derived from the lower bound of the approximate 95 percent confidence limit for 95 percent survival based on a regression analysis of the test data. For convenience in calculating the remaining life in years, a constant K is used rather than A . This constant is related to A by

$$K = \frac{A}{365 \times 10^6} \quad (2.6)$$

In the denominator, 365 converts from days to years, and 10^6 simply reduces the number of digits required to display K.

When calculating the remaining mean life, the constant f is used to modify the constant K. The constant f = the ratio of the mean stress range curve intercept, A', and the allowable stress range curve intercept, A. As previously discussed, the mean stress range curve is simply derived from a regression analysis of the fatigue test data. No modification to the constant K is necessary when calculating the remaining safe life. Thus, when calculating the remaining safe life, $f = 1.0$.

The allowable stress range curve and the mean stress range curve are assumed to be parallel on a log-log plot. Consequently, the slope for both curves is the same. Thus, $b =$ the slope of either curve.

2.5.2.5 Lifetime Average Daily Truck Volume (T_a) Using Figure 5, the lifetime average daily truck volume in the outer lane, T_a , can be determined from the present average daily truck volume in the outer lane, T, the annual growth rate, g, and the present age of the bridge, a.

The present average daily truck volume in the outer lane, T, can be calculated from the ADT at the site as follows:

$$T = (ADT) F_T F_L \quad (2.7)$$

where ADT = present average daily traffic volume (both directions) on the bridge; $F_T =$ fraction of trucks in the traffic. It is suggested [18] that for

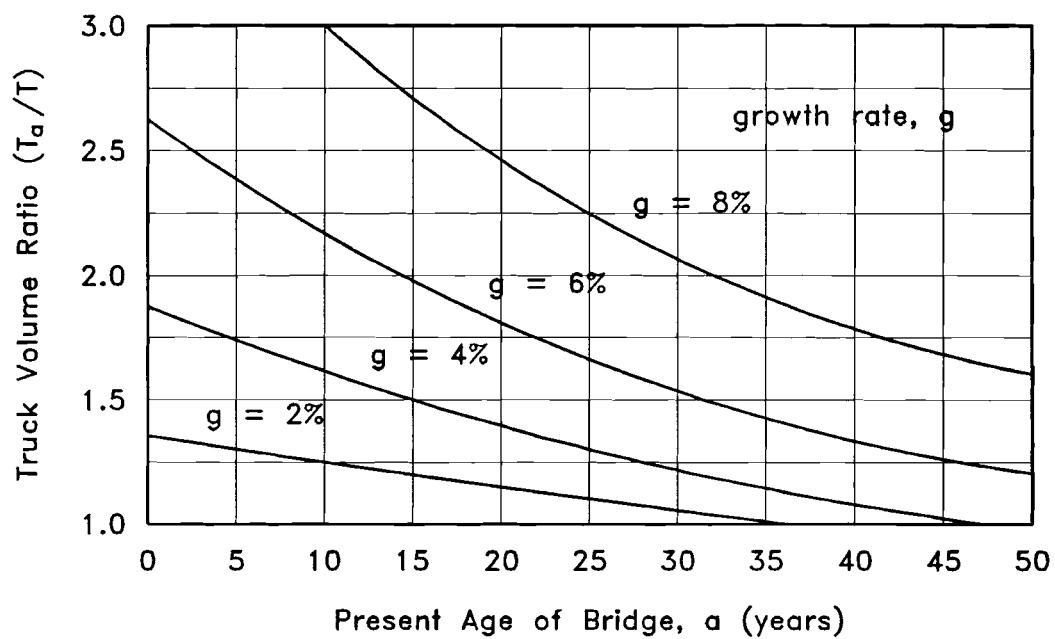


Figure 5. Truck Volume Ratio (T_a/T) [18]

rural Interstate highways $F_T = 0.20$, for rural highways and urban Interstate highways $F_T = 0.15$, and for urban highways $F_T = 0.10$. As determined from Table 2, F_L = fraction of trucks in the outer lane.

The annual growth rate, g , should be estimated by combining a knowledge of local conditions with historical data on growth rates. Table 3 presents growth rate values that were estimated from Annual Average Daily Traffic (AADT) data taken at counting stations throughout the United States between the years 1938 and 1985.

As an example in calculating the lifetime average daily truck volume in the outer lane, T_a , a bridge on a four-lane urban interstate highway is considered. The bridge is 20 years old, and the ADT at the site is 8000 vehicles per day. For urban interstate highways, $F_T = 0.15$, and from Table 2, $F_L = 0.45$ for a four-lane bridge with two-way traffic. Substituting these values into Eq. 2.7

$$T = (\text{ADT}) F_T F_L = (8000)(0.15)(0.45) = 540 \text{ trucks per day}$$

From Table 3, the growth rate, g , at the bridge site is 4.98 percent. For simplicity, the growth rate is rounded to 5.0 percent. Thus, $T = 540$ trucks per day, $g = 5.0$, and $a = 20$ years. Using Figure 5, the truck volume ratio $(T_a/T) = 1.7$ resulting in a lifetime average daily truck volume, $T_a = 918$ trucks per day.

Table 2. Fraction of Trucks in Outer Lane [18]

No. of Lanes	2-Way Traffic	1-Way Traffic
1	-	1.00
2	0.60	0.85
3	0.50	0.80
4	0.45	0.80
5	0.45	0.80
6 or more	0.40	0.80

Table 3. Observed Average Daily Traffic (ADT) Growth Rates [18]

Type of Highway	Rural or Urban	Growth Rate, %
Interstate	rural	4.45
	urban	4.98
U.S. route	rural	2.87
	urban	4.19
State route	rural	3.77
	urban	3.27

CHAPTER III

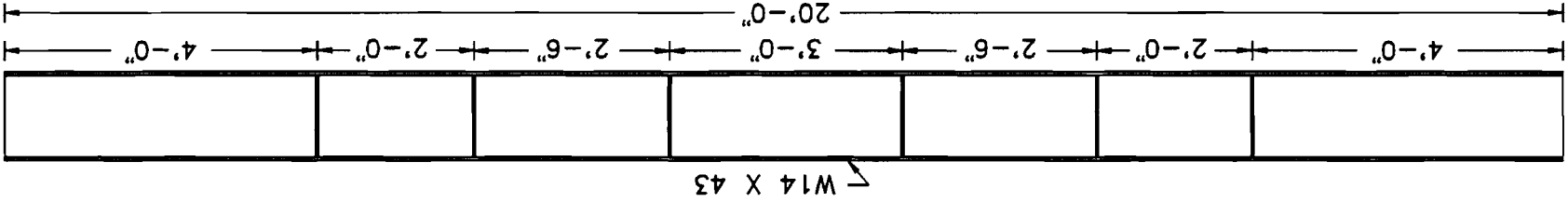
EXPERIMENTAL PROGRAM

3.1 Specimen Preparation

Three specimens were prepared for fatigue testing. All three test specimens were W14 X 43 rolled beams with one-sided transverse stiffeners attached to the web and both flanges. The beam and stiffener material used for fabricating the test specimens was ASTM A36 structural carbon steel. For all specimens, six one-sided transverse stiffeners were attached symmetrically about the midpoint of each beam length where the length of each beam was 20 feet. Attaching the stiffeners in this fashion allowed the fatigue testing of one beam to result in two data points at three different stress ranges for a total of six possible data points per beam. A diagram showing longitudinal dimensions and stiffener locations for a typical test specimen is given in Figure 6. The stiffeners used on the test specimens were steel plates with a width of 3 inches and a thickness of 3/8 inches. The stiffeners were attached to the web and flanges of each beam with 1/4 inch fillet welds. A diagram showing cross-sectional dimensions and weld specifications for a typical test specimen is given in Figure 7.

To provide a basis for comparing test data and to ensure that the test procedures yielded results comparable to results reported in the literature, a control was needed. One of the three test specimens prepared served as the control. The control specimen was prepared by a reputable steel

Figure 6. Longitudinal View of a Typical Test Specimen



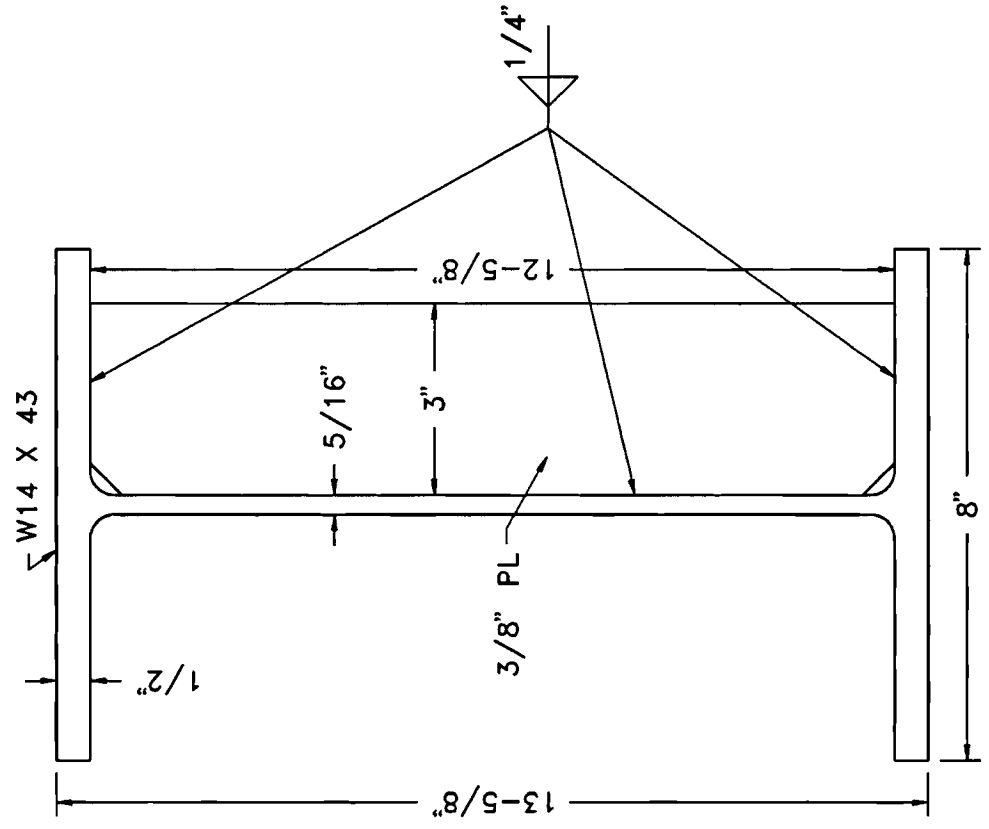


Figure 7. Cross Section of a Typical Test Specimen

fabrication shop. The fabricator was sent the plans and specifications for a typical test specimen. Taking a 20 foot length of a W14 X 43 rolled steel beam, the fabricator attached the one-sided transverse stiffeners by welding to the web and both flanges. The fabricator attached the stiffeners with 1/4 inch fillet welds using the flux cored arc welding (FCAW) process. Because the test data obtained from the control specimen would be compared to the test data obtained from previous tests on stiffener details fabricated with quality welds, it was important for the control specimen to be fabricated with quality welds. Hence, the fabricator was instructed to use normal fabrication techniques, workmanship, and inspection procedure conforming to the requirements of the ANSI/AASHTO/ AWS D1.5 Bridge Welding Code. A typical welded joint made on the control specimen is shown in Figure 8.

The two remaining test specimens were fabricated in the testing laboratory. The completed control specimen along with two 20 foot long W14 X 43 plain rolled steel beams without stiffeners were transported on a trailer from the steel fabrication shop to the testing laboratory. The steel beams obtained from the fabricator were used to make the two remaining test specimens. Additionally, several feet of 3-in. by 3/8-in. flat plate stock needed for fabricating the test specimens were obtained from a local steel supplier, and the welding materials needed for fabricating the test specimens were obtained from a local materials distributor.

The stiffeners for the two remaining test specimens were fabricated from the 3-in. by 3/8-in. flat plate stock. A bandsaw was used to cut the plate into stiffeners that would fit between the top and bottom flanges of each beam. In addition, the corners on the stiffener plates adjacent to the web of each beam were cut at a 3/4-in. by 3/4-in. diagonal. This allowed the stiffeners to be placed against the web of each beam without

fabrication shop. The fabricator was sent the plans and specifications for a typical test specimen. Taking a 20 foot length of a W14 X 43 rolled steel beam, the fabricator attached the one-sided transverse stiffeners by welding to the web and both flanges. The fabricator attached the stiffeners with 1/4 inch fillet welds using the flux cored arc welding (FCAW) process. Because the test data obtained from the control specimen would be compared to the test data obtained from previous tests on stiffener details fabricated with quality welds, it was important for the control specimen to be fabricated with quality welds. Hence, the fabricator was instructed to use normal fabrication techniques, workmanship, and inspection procedure conforming to the requirements of the ANSI/AASHTO/ AWS D1.5 Bridge Welding Code. A typical welded joint made on the control specimen is shown in Figure 8.

The two remaining test specimens were fabricated in the testing laboratory. The completed control specimen along with two 20 foot long W14 X 43 plain rolled steel beams without stiffeners were transported on a trailer from the steel fabrication shop to the testing laboratory. The steel beams obtained from the fabricator were used to make the two remaining test specimens. Additionally, several feet of 3-in. by 3/8-in. flat plate stock needed for fabricating the test specimens were obtained from a local steel supplier, and the welding materials needed for fabricating the test specimens were obtained from a local materials distributor.

The stiffeners for the two remaining test specimens were fabricated from the 3-in. by 3/8-in. flat plate stock. A bandsaw was used to cut the plate into stiffeners that would fit between the top and bottom flanges of each beam. In addition, the corners on the stiffener plates adjacent to the web of each beam were cut at a 3/4-in. by 3/4-in. diagonal. This allowed the stiffeners to be placed against the web of each beam without



Figure 8. A Typical Welded Joint on the Control Specimen

interference from the rounded fillets occurring at the intersections of the web and flanges. Using a bench grinder, the top and bottom edges of the stiffener plates were ground slightly allowing them to fit firmly against the web and flanges of each beam.

After fabricating the stiffener plates, they were located along the two 20 foot long plain rolled beams. The stiffener locations were measured from the midpoint of each beam outward. The locations were identified along the bottom flange of each beam using a hole punch and a colored marker. The stiffener plates were made square with the web and flanges of each beam using a framing square and a carpenter's level.

With the stiffener plates in place, they were secured by welding both sides of the plates to the web and flanges of each beam. The welds were manually produced using the shielded metal arc welding (SMAW) process. Figure 9 shows the welding equipment used along side one of the test specimens being welded. As shown in Figure 9, welding was performed while the webs of the beams were in a vertical upright position. Welding was performed with the beams in this position to simulate field welding a girder detail on an existing steel bridge. The power source used for welding was operated at 200 amps of alternating current (AC), and the electrodes used for welding were 1/8-in. diameter solid metal rods designated as E6011 which are known for their excessive hydrogen content.

To properly represent the field welds being evaluated, the welding performed on the two specimens fabricated in the laboratory was to be sufficiently poor as to produce substandard welds. Poor quality welds containing excessive discontinuities were obtained by simply using substandard welding techniques. Welding with excessive arc current and with electrodes high in hydrogen content aided in producing substandard



Figure 9. Welding a Test Specimen

welds. The failure to preheat also encouraged welds with poor quality. Furthermore, the laboratory technician responsible for welding the details was instructed to produce poor quality welds by moving the electrode in and out at several locations. Manipulating the electrode in this manner was intended to simulate the movement that would occur while welding to a bridge with traffic present. The combination of the poor welding techniques employed resulted in welds with excessive discontinuities. A typical welded joint made on one of the test specimens fabricated in the laboratory is shown in Figure 10.

On one of the test specimens fabricated with poor quality welds, an attempt was made to repair a welded joint at one of the stiffener details. The stiffener detail selected was located closest to the midpoint of the beam where stress range would be the highest. Furthermore, the welded joint selected was located at the intersection of the stiffener plate and the tension flange of the beam where obvious undercut was present in the flange. Repair was accomplished by grinding along the fillet welds joining both sides of the stiffener plate to the tension flange. Both weld material and flange material were reduced by grinding until undercut was removed and a smooth transition was obtained. This helped to minimize stress concentrations and reduce weld discontinuities. By grinding, the flange thickness was reduced by a maximum of 0.044 inches. The ground joint is shown in Figure 11. Grinding was performed using both a rotary burr grinder and a disc grinder. The pneumatically powered rotary burr grinder was used to quickly remove the majority of unwanted material. The electrically powered disc grinder was used to smooth out scratches left by the rotary burr grinder. Completely grinding the welded joint took approximately 15 minutes.

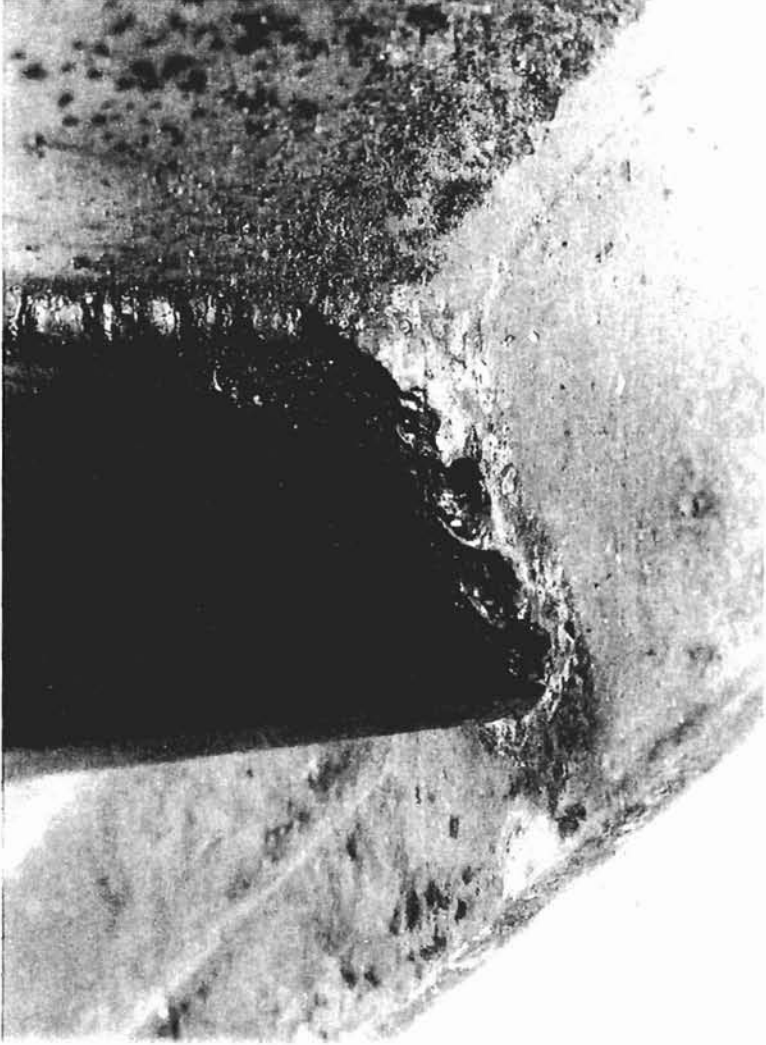


Figure 10. A Typical Welded Joint with Substandard Welds



Figure 11. Repaired Joint

Before testing, the three specimens were fitted with strain gages so that actual stress ranges could be determined. Both 350 ohm and 120 ohm strain gages were used. Strain gages were placed along the inside of the tension flange of each beam. More specifically, the strain gages were placed approximately 4 inches away from the stiffener details and approximately 1 inch from the edges of the tension flange. The strain gages were placed on each side of the tension flange. The diagram in Figure 12 shows the strain gage configuration at a stiffener detail.

3.2 Test Setup

All specimens were tested on simple supports. The rotational freedom of the simple supports was provided by a cylindrical roller trapped between two thick plates. The plates were rounded to accommodate the cylindrical roller. The rounded plates and the cylindrical roller were thoroughly coated with grease to reduce friction. To prevent unwanted movement of the test specimen, threaded fasteners held the test specimen firmly against the simple supports. Figure 13 shows a side view of the simple supports. All specimens were tested on an 18 foot span with two-point loading where the distance between the load points was 5 feet. The load configuration is shown in Figure 14. At the load points, rotational freedom was allowed by a rotational mechanism similar to that used on the simple supports. Loads were applied by a hydraulic actuator and were distributed to the two locations on the test specimens through a spreader beam. The servo-controlled hydraulic actuator operated between 0.6 and 2.7 cycles of load application per second with a maximum capacity of 50 kips. The servos were commanded by an electronic control unit near the test site, and the

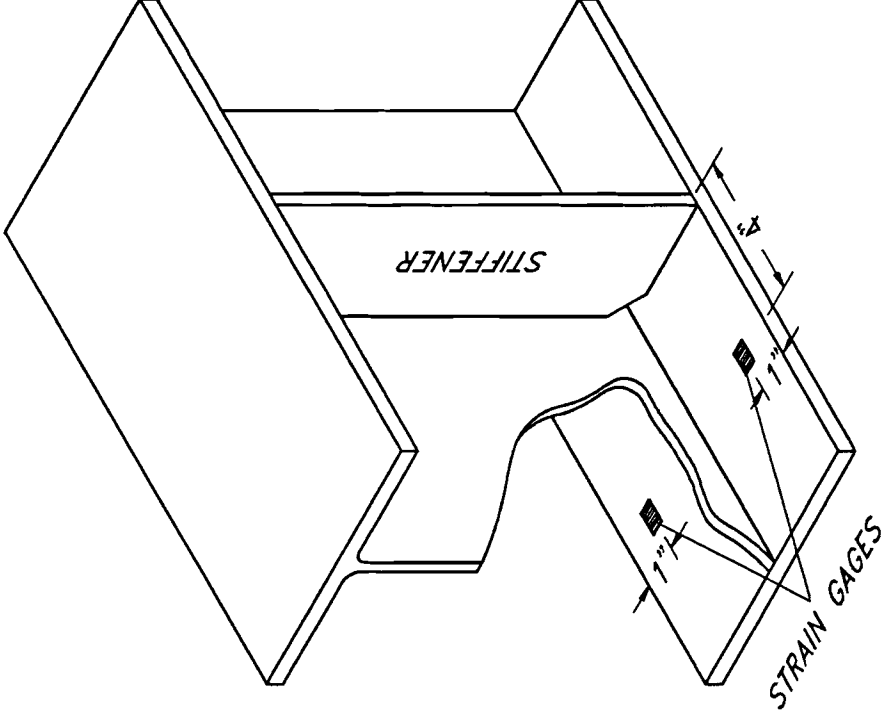


Figure 12. Strain Gage Configuration

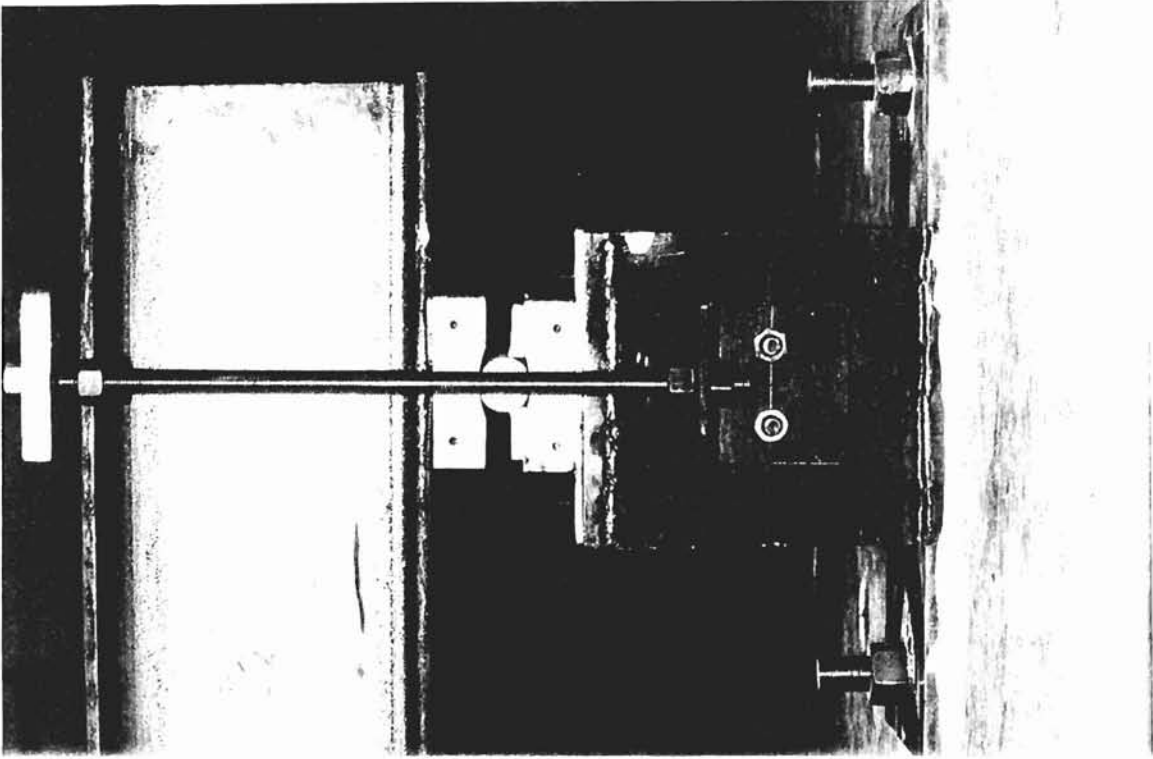
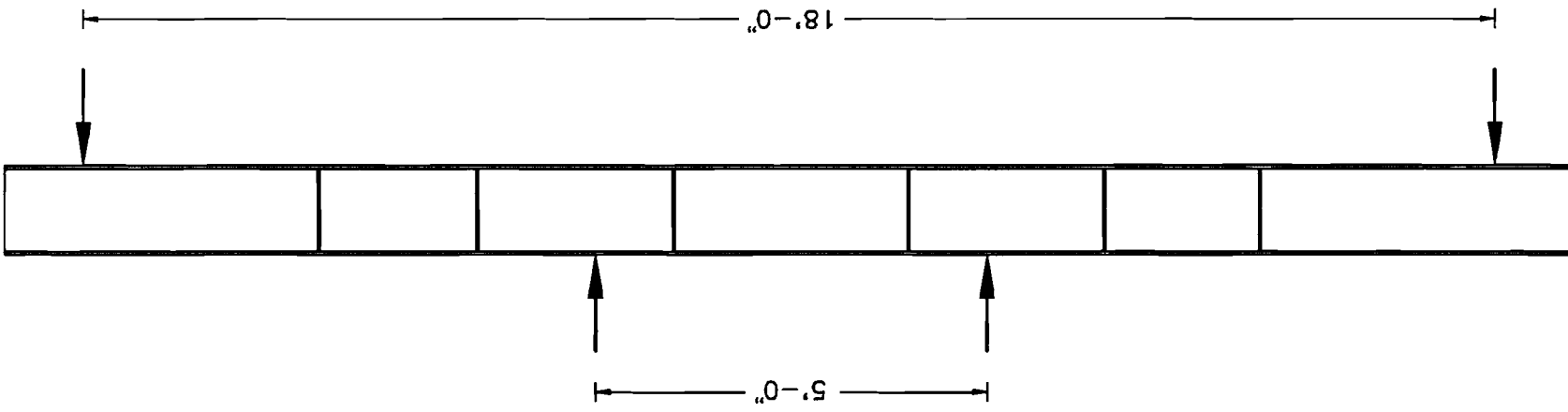


Figure 13. Simple Support

Figure 14. Load Configuration on Test Specimen



actuator was activated by a hydraulic pump located beyond the test site. The hydraulic actuator was supported above by a steel test frame. The test frame and the simple supports were securely fastened to a reinforced concrete reaction floor. For safety, side rollers attached to the columns of the test frame were positioned against the web of the spreader beam to prevent possible bucking. The test setup is shown in Figure 15. All components of the test setup such as the test frame, the simple supports, and the spreader beam were designed to withstand the numerous load cycles required to fatigue test the three specimens.

3.3 Test Procedures

Each test specimen was carried from the fabrication site to the test site and manipulated at the test site with an overhead crane. The manual controls on the overhead crane allowed each test specimen to be carefully placed into position without harming the stiffener details or strain gages. With a test specimen positioned between the simple supports and the spreader beam, the web of the test specimen was carefully aligned with the center of the load points and all restraining fasteners were tightened. Once the specimen was secured, the electronic unit commanding the servos and the hydraulic pump activating the actuator were powered.

Before beginning the fatigue test on each specimen, a static load test was performed. These tests were performed while monitoring the strain gages along the tension flange of each specimen. The strain gages were monitored using a Wheatstone bridge and a switching unit. For each static load test, the load was increased by increments of 5 to 10 kips up to a peak value. Once the peak value was reached, the load was decreased by

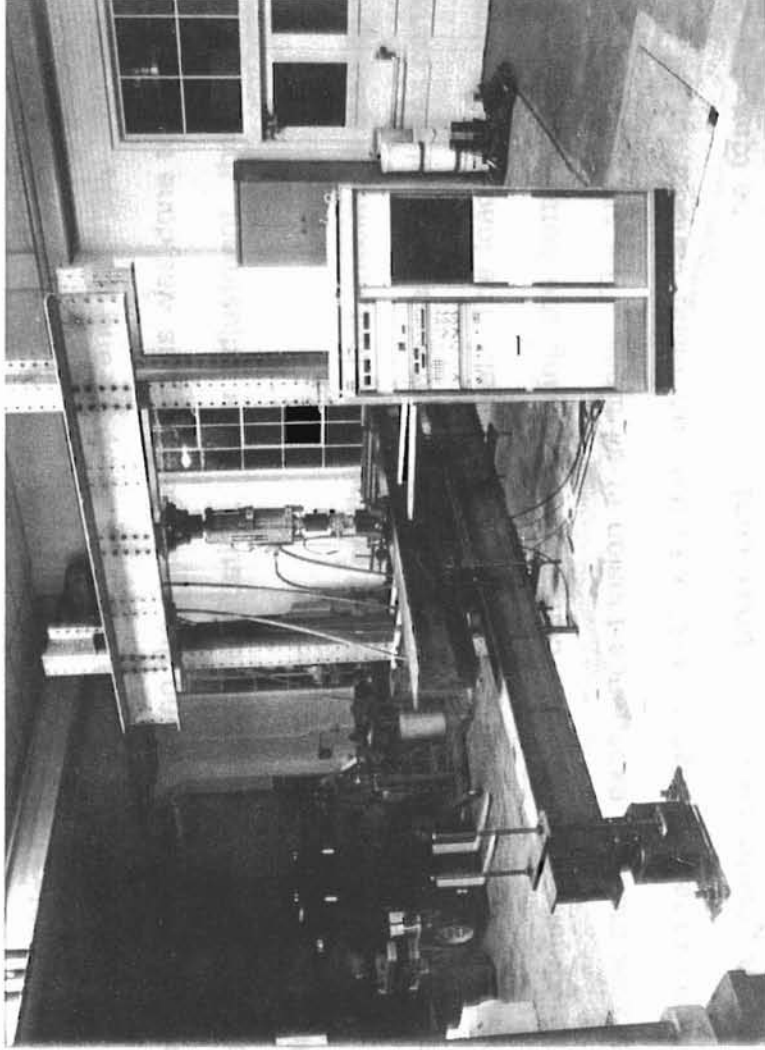


Figure 15. Test Setup

increments of 5 to 10 kips. Strains were recorded for each increment of load and the corresponding stresses were calculated. To determine if the test specimen was properly aligned, the actual stresses occurring in the test specimen were compared to theoretical stresses, and the strains occurring on each side of the tension flange were compared to each other. If improper alignment was suspected, the test specimen was simply readjusted until favorable strains were measured.

On occasion, the fatigue test was stopped, and the static load test was performed while monitoring the strain gages. This was done to determine if the test specimen needed readjusting. After adjustment, the fatigue test was continued.

Fatigue testing was performed on the three test specimens starting with the control specimen. For all test specimens, the load applied was constant amplitude cyclic loading without stress reversal. The load applied through the hydraulic actuator was compressive causing the bottom flange of the test specimens to experience tension at all times. The stress range at the stiffener-to-tension flange weld was the controlling variable for all fatigue tests. A counter on the electronic control unit recorded the total number of load cycles each test specimen experienced. Fatigue testing on each specimen continued until a crack occurring at stiffener detail reduced beam stiffness and allowed for relatively large deflections. The electronic control unit stopped the hydraulic pump when internal circuitry sensed the large displacements of the hydraulic actuator. After each crack, the stress range at stiffener-to-tension flange weld and the total number of load cycles to failure were recorded.

After failure, fatigue testing was continued to obtain cracks at other stiffener details by repairing the flange at the cracked stiffener detail. The

repairs were accomplished by splicing across the cracked region. Splice plates with a thickness of 3/8-in. were bolted above and below the tension flange with 3/4-in. diameter A325 bolts. The bolts were accommodated by drilling holes through the tension flange and splice plates. Because of the nature of the fatigue loading, the splice plate details were designed as slip-critical connections requiring several bolts on each side of a crack. A typical splice plate detail is shown in Figure 16.

3.4 Results and Discussion

The data acquired from fatigue testing the three specimens included the total number of load cycles, N , each stiffener detail sustained until failure and the corresponding stress range, S_r , occurring at each of the failed stiffener details. The stress range was calculated at the fillet weld joining the stiffener to the tension flange. The bending stress formula derived from theoretical structural analysis was used to calculate the stress ranges.

The stress range values calculated from the bending stress formula were validated by comparing them to the stress range values calculated from strain gage readings. As previously discussed, strain gages were monitored while performing static load tests. For all test specimens, the stress range values calculated from strain gage readings varied less than 3.8 percent from the stress range values calculated from the bending stress formula. It is therefore reasonable to assume that the stress range values calculated from the bending stress formula are reliable. In addition, strains recorded near opposite edges of the tension flange at the same locations along the span varied less than 3.7 percent for all test specimens. Hence, twisting of the test specimens was minor and torsion need not be considered. These

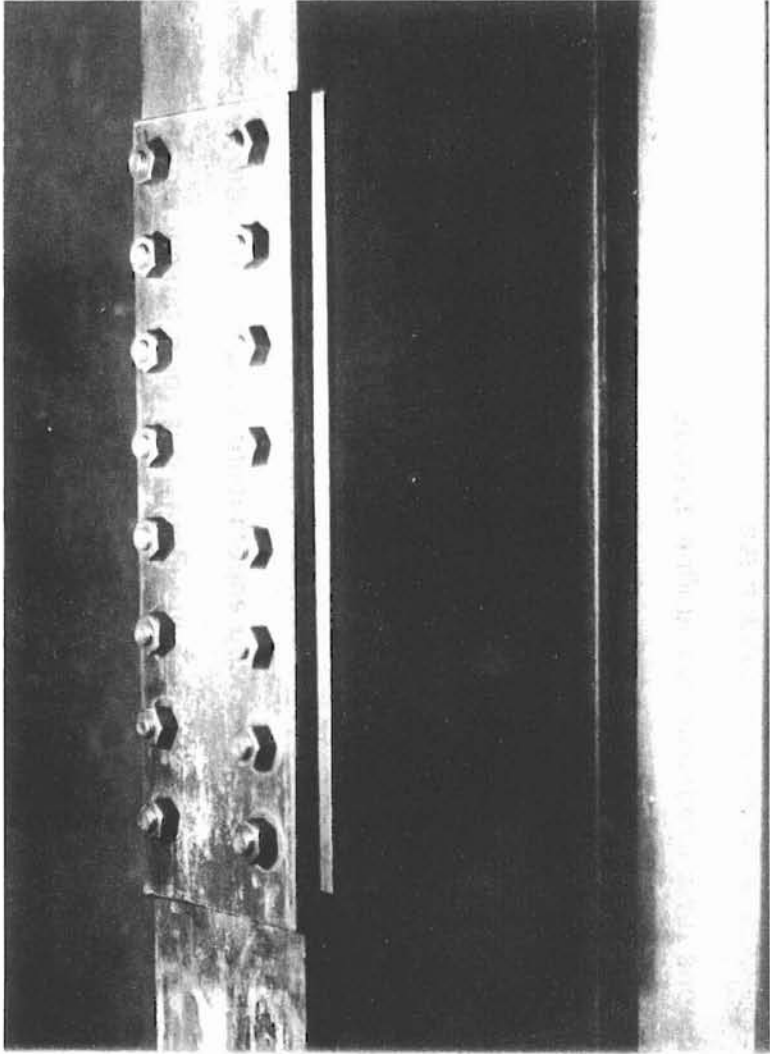


Figure 16. Splice Plate Detail

results were observed throughout the fatigue tests.

All failures occurring in the fatigue tests were the result of a crack initiating and growing adjacent to the fillet weld joining the stiffener to the tension flange. A typical failure is shown in Figure 17. Beams reached the end of their fatigue life when the crack had destroyed most of the tension flange and deflections had become large. Some of the cracks propagated up into the web of the test specimens. A typical crack starting from a surface discontinuity at the toe of the fillet weld is shown in Figure 18. The cross-sectional view presented in Figure 18 is for a typical stiffener detail on a test specimen fabricated with substandard welds. The region where slow growth prevailed over a large portion of the life is apparent from the smooth fracture appearance [10].

The load cycles to failure and the stress range data obtained from each test specimen are shown in Table 4. The results for the control specimen are in close agreement with those presented by Fisher et al. [10]. Recalling from an earlier discussion, data were accumulated by Fisher et al. in numerous tests examining the fatigue strength of stiffener details. In Figure 19, the data obtained from fatigue testing the control specimen is compared to the curve generated from a linear regression analysis of Fisher's data. The close agreement between the results for the control specimen and Fisher's results indicates the reliability of the test setup and the test procedures followed in this study.

The results obtained from fatigue testing the stiffener details fabricated with poor quality welds are presented in Figure 20. Included in Figure 20 are the data points, the curve generated from a linear regression analysis of the data, and the lower bound curve derived from the approximate 95 percent confidence limit for the data. The fatigue limit for the stiffener



Figure 17. A Typical Crack at a Stiffener Detail

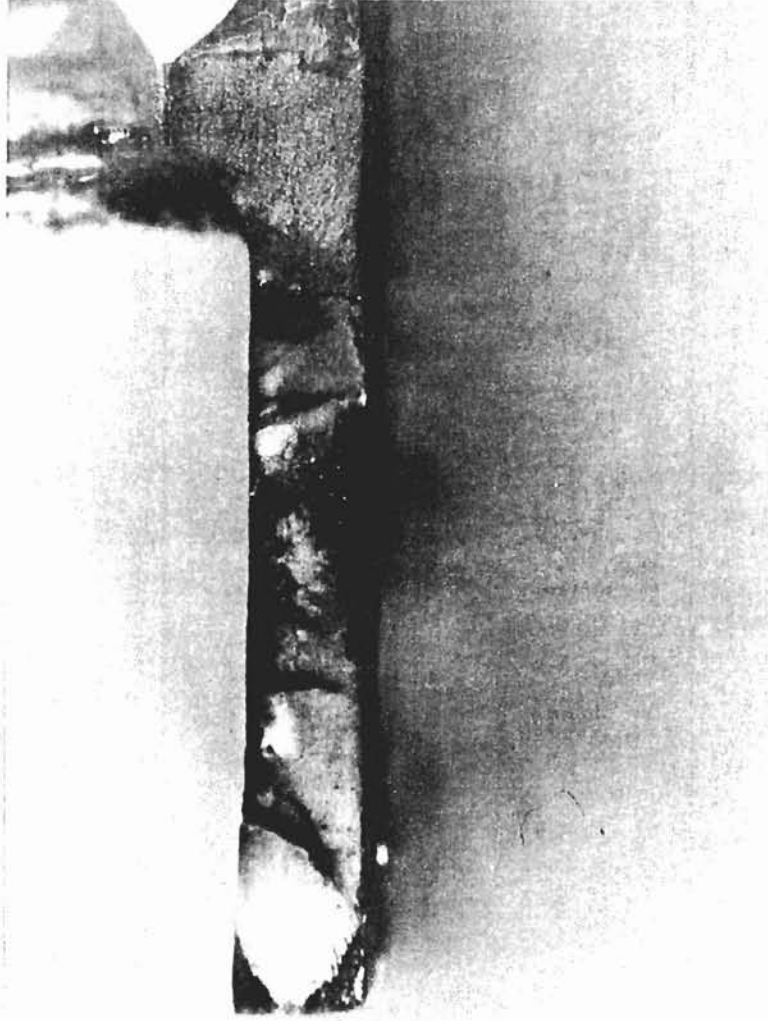


Figure 18. Crack Surface at a Stiffener Detail

Table 4. Fatigue Test Data

Specimen No.	Stress Range, S_r (ksi)	Cycles to Failure, N
1 - control	27.6	322510
	27.6	332410
	21.2	828170
	21.2	842630
2	27.6	59260
	27.6	80320
	21.2	104650
	21.2	549150
	12.7	2105650
3	17.2	625700
	17.2	625700
	13.2	2201510
	13.2	4964770 *

* no failure

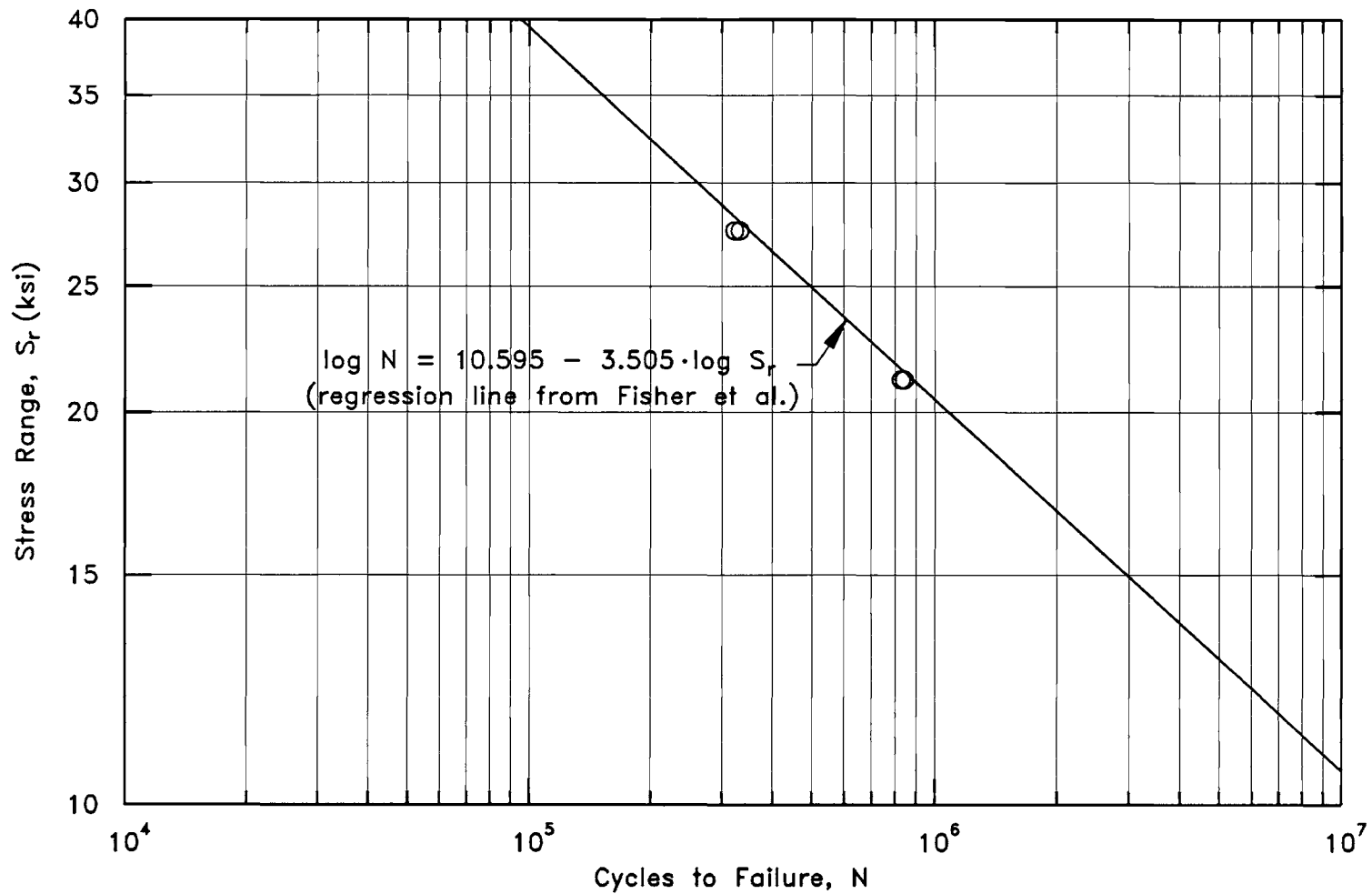


Figure 19. Comparison of the Control Specimen Test Data and the Fatigue Curve Generated by Fisher et al.

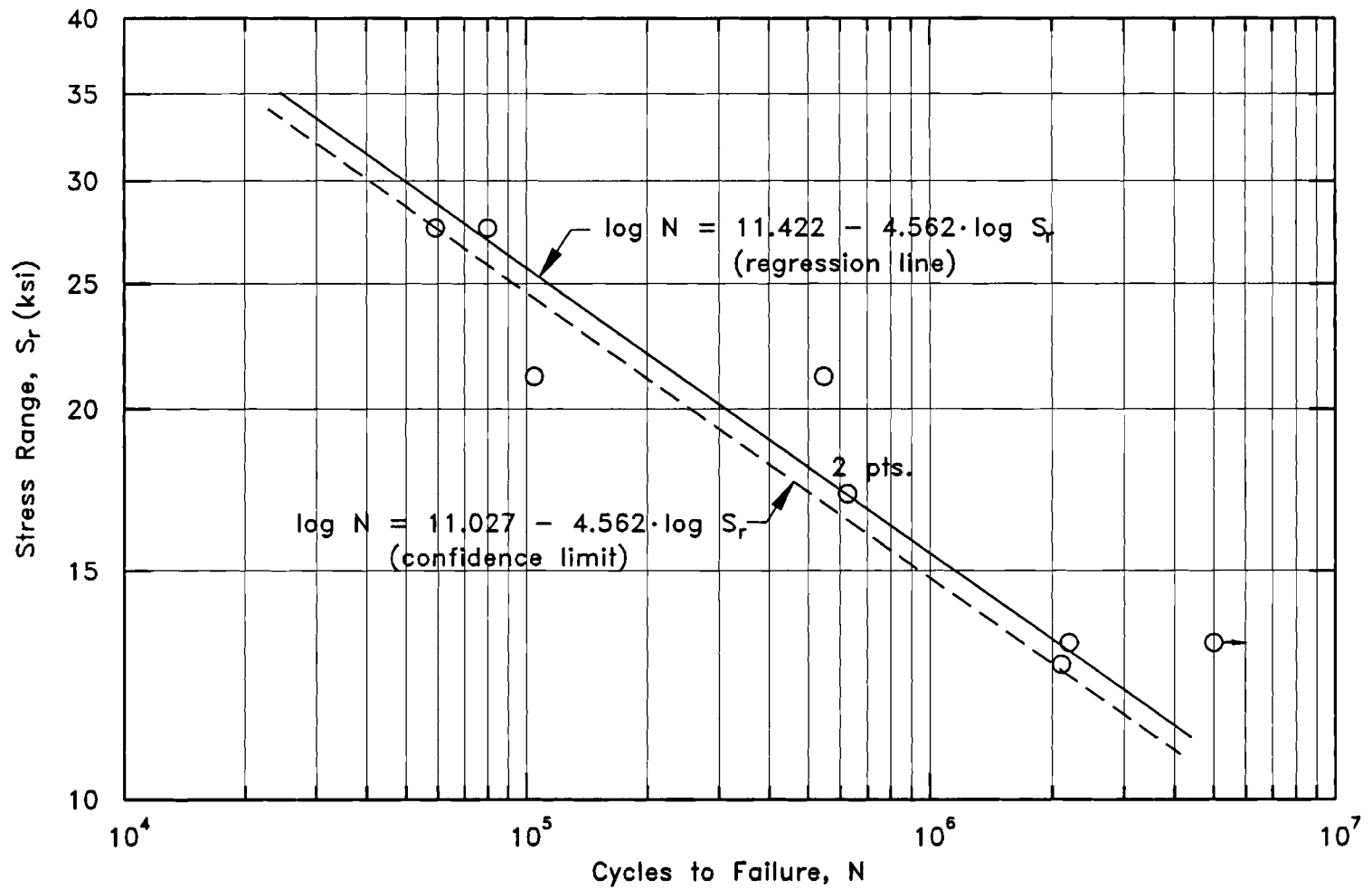


Figure 20. Plot of the Test Data for the Stiffener Details with Substandard Welds

details with substandard welds was not clearly defined; however, one stiffener detail sustained over 4.9 million load cycles at a stress range of 13.2 ksi without failure or visible crack growth. Fatigue testing of the specimen containing this stiffener detail was stopped as a result of fatigue cracks occurring elsewhere along the span.

In Figure 21, the data for the stiffener details having poor weld quality are plotted along with the AASHTO fatigue curves for Category C and D details. Also shown in Figure 21 is the lower bound fatigue curve derived from the approximate 95 percent confidence limit for the test data. Most of the test data for the stiffener details having poor weld quality fall below the fatigue curve for an AASHTO Category C detail. In further comparison, the slope of the fatigue curve for the stiffener details with poor weld quality is 4.562 whereas the slope of the fatigue curve for an AASHTO Category C detail is 3.0. The lower bound fatigue curve derived from the approximate 95 percent confidence limit for the test data intersects the fatigue curve for an AASHTO Category C detail at approximately 12.0 ksi. Thus, the fatigue strength of stiffener details fabricated with substandard welds is lower than the fatigue strength of AASHTO Category C details at stress ranges greater than 12.0 ksi. Recalling that the lowest stress range examined in the fatigue tests was 12.7 ksi indicates further testing at lower stress ranges may be needed.

As previously discussed, an attempt was made to repair one of the stiffener details on a test specimen fabricated with substandard welds. On this test specimen, the repaired stiffener detail and one other stiffener detail experienced the same stress range of 17.2 ksi. Ironically, both specimens failed at the same number of load cycles indicating the repair was ineffective. These test results may be explained by relying on a

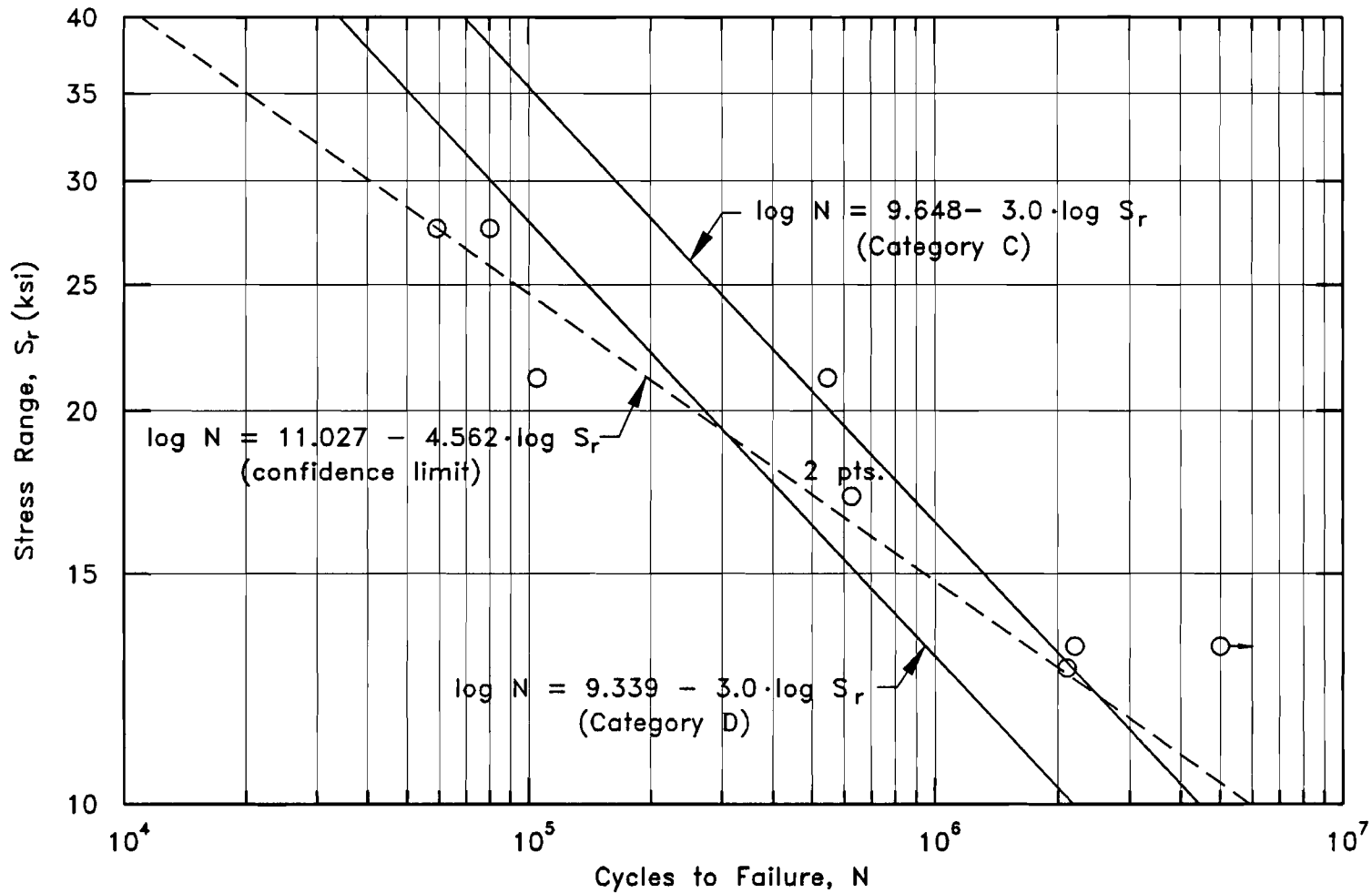


Figure 21. Comparison of the Test Data to AASHTO Fatigue Curves for Category C and D Details

investigation by Gregory et al. [13]. Recalling from earlier discussion, Gregory conducted fatigue tests on stiffener details that were repaired by rotary burr and disc grinding. Although Gregory obtained favorable results showing increases in fatigue strength, Gregory's tests involved stress ranges much lower than 17.2 ksi. Thus, it seems reasonable to assume the repairs on the test specimen would have been more effective on a stiffener detail subjected to a lower stress range.

CHAPTER IV

ESTIMATE OF REMAINING FATIGUE LIFE

An Estimate of the remaining fatigue life of the U.S. Highway 69 bridge crossing the South Canadian River is based on the results of the fatigue tests on stiffener details fabricated with substandard welds. The results of the fatigue tests on stiffener details fabricated with substandard welds were discussed in Section 3.4. In Figure 20 of Section 3.4, the curve generated from a linear regression analysis of the fatigue test data, and the lower bound curve derived from the approximate 95 percent confidence limit for the fatigue test data were presented. The logarithmic equations defining these curves were also presented in Figure 20. The slope and intercept values shown in these equations are used below to calculate the remaining fatigue life of the U.S. Highway 69 bridge.

The remaining fatigue life calculation for the U.S. Highway 69 bridge follows from the fatigue evaluation procedures presented in Section 2.5. In Section 2.5, two different procedures for estimating the remaining fatigue life of a bridge detail are presented. The two procedures presented are identified as remaining mean life and remaining safe life. The remaining mean life calculation for the U.S. Highway 69 bridge uses the mean stress range curve which is equivalent to the fatigue curve generated from the linear regression analysis of the test data shown in Figure 20. The remaining safe life calculation for the U.S. Highway 69 bridge uses the allowable stress range curve which is equivalent to the lower bound fatigue

curve derived from the approximate 95 percent confidence limit for the test data shown in Figure 20. As given in Section 2.5, the remaining mean life and the remaining safe life are calculated from Eq. 2.1.

$$Y_f = \frac{f K X 10^6}{T_a C (R_s S_r)^b} - a$$

The effective stress range, S_r , at specific locations along the bridge is calculated from stress-range histograms using Eq. 2.2.

$$S_r = (\sum p_i S_{ri}^3)^{1/3}$$

Stress-range histograms were obtained from field measurements on the bridge under normal traffic.

The effective stress range occurring at the most critical stiffener detail on the U.S. Highway 69 bridge was determined from a finite element model of the bridge structure. Following procedures similar to those discussed in Section 2.4.2., the finite element model of the bridge structure was calibrated using the effective stress ranges measured at specific locations along the bridge. The calibrated model was then examined to find the effective stress range at the most critical stiffener detail on the bridge. The effective stress range, S_r , at the most critical stiffener detail was found to be 0.96 ksi.

To determine the remaining safe life, the reliability factor, R_s , is calculated from equation 2.3,

$$R_s = R_{s0} (F_{s1})$$

Because the effective stress range, S_r , was determined from stress-range histograms, $F_{s1} = 0.85$. Because the most critical stiffener detail is attached to a redundant member, $R_{s0} = 1.35$. Substituting these values into Eq. 2.3.

$$R_s = 1.35 (0.85) = 1.15$$

To determine the remaining mean life, the reliability factor, $R_s = 1.0$

The stress cycles per truck passage, C , is determined from Section 2.5.2.3. The U.S. Highway 69 bridge consists of continuous girders with spans greater than 40-feet. Thus, the stress cycles per truck passage, C , has a value of 1.0.

To determine the fatigue curve constants (K , b , and f), the fatigue curves presented in Figure 20 are used. From Figure 20, the equation defining the lower bound curve derived from the 95 percent confidence limit for the test data is given in the form of Eq. 2.5.

$$\log N = \log A - b \cdot \log S_r$$

where $\log A$ has a value of 11.027, and A has a value of 1.064×10^{11} . Using the intercept, A the fatigue curve constant K is calculated from Eq. 2.6.

$$K = \frac{A}{365 \times 10^6} = \frac{1.064 \times 10^{11}}{365 \times 10^6} = 292$$

Also from Figure 20, the slope b has a value of 4.562.

To compute the remaining safe life, $f = 1.0$. To compute the remaining mean life, $f =$ the ratio of the mean stress range curve intercept, A' , and

the allowable stress range curve intercept, A . As discussed above, the mean stress range curve and the allowable stress range curve are equivalent to the curves shown in Figure 20. The intercept A' for the mean stress range curve has a value of 2.642×10^{11} . Thus, the ratio, f , used to compute the remaining mean life is determined as

$$f = \frac{2.642 \times 10^{11}}{1.064 \times 10^{11}} = 2.48$$

From Section 2.5.2.5, the lifetime average daily truck volume, T_a , is determined from the present average daily truck volume in outer lane, T , the annual growth rate, g , and the present age of the bridge, a .

The present average daily truck volume in the outer lane, T , is calculated from Eq 2.7,

$$T = (ADT) F_T F_L$$

As determined from the bridge design data provided by ODOT, the present average daily traffic volume on the bridge is 9700 vehicles per day. Furthermore, U.S. Highway 69 is a rural highway supporting 2-way traffic in 4 lanes. Thus, the fraction of trucks in the traffic, F_T , has a value of 0.15, and the fraction of trucks in the outer lane, F_L , as determined from Table 2 has a value of 0.45. These values are substituted into Eq. 2.7.

$$T = (ADT) F_T F_L = (9700)(0.15)(0.45) = 655 \text{ trucks per day}$$

The annual growth rate is determined from Table 3. For a rural U.S. route such as U.S. Highway 69, the growth rate value taken from Table 3 is 2.87. This value is rounded up making the annual growth rate, $g = 3.0$.

The U.S. Highway 69 bridge was originally constructed in 1963 making the present age of the bridge, $a = 32$ years.

Applying the values determined for T , g , and a to Figure 5 gives a truck volume ratio (T_a/T) of approximately 1.2 and a lifetime average daily truck volume, T_a , of approximately 786 trucks per day.

The final step in the fatigue evaluation procedures is to calculate the remaining mean life and the remaining safe life. The variables determined above for the U.S. Highway 69 bridge are substituted into Eq 2.1.

$$Y_f = \frac{f K \times 10^6}{T_a C (R_s S_r)^b} - a$$

The remaining safe life is

$$Y_f = \frac{1.0 \cdot 292 \times 10^6}{786 \cdot 1.0 (1.15 \cdot 0.96)^{4.562}} - 32 = 236525 \text{ years}$$

The remaining mean life is

$$Y_f = \frac{2.48 \cdot 292 \times 10^6}{786 \cdot 1.0 (1.0 \cdot 0.96)^{4.562}} - 32 = 1109885 \text{ years}$$

From the calculations above, it is clear that the remaining fatigue life of the U.S. Highway 69 bridge crossing the South Canadian River far exceeds the design life. For comparison, when the remaining safe life of the U.S.

Highway 69 bridge is calculated using the allowable stress range curves for AASHTO Category C and D details, the results are 11485 years and 5623 years, respectively. Furthermore, if the total safe life desired is 100 years, the stress range allowed on the U.S. Highway 69 bridge at the most critical detail is 3.68 ksi based on the AASHTO Category D fatigue curve.

CHAPTER V

SUMMARY AND CONCLUSIONS

5.1 Summary

Recent widening of the U.S. Highway 69 bridge crossing the South Canadian River required the addition of several stiffener details. Unfortunately, the stiffener details were fabricated with substandard welds. After completing the new construction, it was suspected that the substandard welding had reduced the remaining fatigue life of the bridge.

The purpose of this study was to evaluate the remaining fatigue life of the U.S. Highway 69 bridge using data obtained from fatigue tests on stiffener details fabricated with substandard welds. In addition, a suitable method of repairing the substandard welds at the stiffener details was to be investigated.

Fatigue tests were conducted on three W14 X 43 rolled steel beams with one-sided transverse stiffeners. The stiffeners were fabricated from 3-in. by 3/8-in. steel plate. The beam and stiffener material was A36 structural carbon steel. The stiffener plates were welded to the web and both flanges of each beam. On one of the test specimens, the control specimen, the stiffener details were fabricated with quality welds. On the remaining two test specimens the stiffener details were purposely fabricated with substandard welds. An attempt was made to repair one of the stiffener details fabricated with substandard welds by rotary burr and disc grinding.

5.2 Conclusions

The following Conclusions are drawn from the results of this study:

1. The fatigue strength of stiffener details is significantly reduced by the presence of weld defects at stress ranges greater than 12.0 ksi.
2. Substandard welds reduce the fatigue strength of stiffener details below the fatigue strength of AASHTO Category C details at stress ranges greater than 12.0 ksi.
3. As indicated from both the literature and the test results, repairing substandard welds at stiffener details by rotary burr and disc grinding is not an effective means of prolonging fatigue life at high stress ranges. However, favorable results may be achieved at low stress ranges.
4. The remaining fatigue life of the U.S. Highway 69 bridge far exceeds the design life.

REFERENCES

- [1] AASHTO *Standard Specifications for Highway Bridges*, American Association of State Highway and Transportation Officials (1990)
- [2] American Welding Society, *Welding Technology Handbook, Vol. 1*. Miami: American Welding Society, 1987
- [3] American Welding Society, *ANSI/AWS Structural Welding Code*. Miami: American Welding Society, 1990
- [4] American Welding Society. *Welding Technology Handbook, Vol. 2*. Miami: American Welding Society, 1991
- [5] Barton, F. W. and McKeel, W. T., "Development of an Improved Capability for Predicting the Response of Highway Bridges." Virginia Highway and Transportation Research Council, VHTRC 86-R45, June 1986.
- [6] Buckle, I. G., Dickson, A. R., and Phillips, M. H., "Ultimate Strength of Three Reinforced Concrete Bridges." International Conference on Short and Medium Span Bridges, Toronto, 1982.
- [7] Burdette, E. G. and Goodpasture, D. W., "Full Scale Bridge Testing: An Evaluation of Bridge Design Criteria." University of Tennessee, December 1971.
- [8] Burdette, E. G. and Goodpasture, D. W., "Correlation of Bridge Load Capacity Estimates with Test Data." *NCHRP Report 306*, (1988) 75 pp.
- [9] Fisher, J. W., Frank, K. H., Hirt, M. A., and McNamee, B. M., "Effect of Weldments on the Fatigue Strength of Steel Beams." *NCHRP Report 102*, (1970) 114 pp.

- [10] Fisher, J. W., Albrecht, P. A., Yen, B. T., Klingerman, D. J., and McNamee, B. M., "Fatigue Strength of Steel Beams with Welded Stiffeners and Attachments." *NCHRP Report 147* (1974) 85 pp.
- [11] Fisher J. W., Pense A. W., Hausammann H., and Sullivan M. D., "Detection and Repair of Fatigue Damage in Welded Highway Bridges." *NCHRP Report 206*, (1979) 85 pp.
- [12] Fisher, J. W., and Keating, P. B., "Evaluation of Fatigue Tests and Design Criteria on Welded Details." *NCHRP Report 286*, (1986) 66 pp.
- [13] Gregory, N., Graham, S., and Woodley, C., "Welded Repair of Cracks in Steel Bridge Members." *NCHRP Report 321*, (1989) 46 pp.
- [14] Gurney, T. R., "Fatigue Strength of Beams with Stiffeners Welded to the Tension Flange." *British Welding Journal*, (Sep. 1960) p. 569.
- [15] Gurney, T. R., "Fatigue of Welded Structures." 2nd ed., Cambridge: University Press, 1979, pp. 156-173.
- [16] Highway Research Board, "The AASHO Road Test: Report 4 - Bridge Research," Highway Research Board, (1962)
- [17] Minner, H. H. and Seeger, T., "Improvement of Fatigue Life of Welded Beams by TIG-Dressing." Proc., IABSE Colloquium-Lausanne, Fatigue of Steel and Concrete Structures, (1982) pp. 385-392.
- [18] Moses, F., Schilling, C. G., and Raju, K. S., "Fatigue Evaluation Procedures For Steel Bridges." *NCHRP Report 299*, (1987) 94 pp.
- [19] Nowak A. S., *Bridge Evaluation, Repair and Rehabilitation*. Kluwer Academic Press, 1990, p. 371.
- [20] Rodgerson J. H., *Quality Assurance of Welded Construction*. New York: Elsevier Science Publisher, 1983, pp. 115-131.
- [21] Tsai, C. L., and Tsai, M. J., "Significance of Weld Undercut in Design of Fillet Welded T-Joints." *Welding Journal*, Vol. 63, No. 2 (Feb. 1984), pp. 64s-70s

- [22] Viest, I. M., "Review of Research on Composite Steel-Concrete Beams." *Journal of the Structural Division, ASCE*, Vol. 86, No. ST6, June 1960.

VITA

Paul G. Poynter

Candidate for the Degree of

Master of Science

Thesis: THE FATIGUE STRENGTH OF STIFFENER DETAILS FABRICATED
WITH SUBSTANDARD WELDS

Major Field: Civil Engineering

Biographical:

Personal Data: Born in Midwest City, Oklahoma, On June 3, 1971,
the son of Byron C. and Dianne R. Poynter.

Education: Graduated from Harrah High School, Harrah, Oklahoma, in
May 1989; received the Bachelor of Science degree in Civil
Engineering from Oklahoma State University, Stillwater,
Oklahoma in December, 1993; completed the requirements for
the Master of Science degree at Oklahoma State University in
May, 1995.

Experience: Research Assistant, School of Civil Engineering,
Oklahoma State University, May, 1994, to May, 1995;
Engineer's Assistant, Stillwater Engineering and Consulting
Inc., May, 1993, to May, 1995; Engineer's Assistant, Enogex
Inc., Engineering and Construction Department, summer of
1991 and 1992; Surveyor's Assistant, Oklahoma Department
of Transportation, summer of 1990.